Débora Vale Magalhães

Licenciado em Ciências de Engenharia de Micro e Nanotecnologia

Synthesis of Inorganic Halide Perovskite Quantum Dots for Photoluminescence Applications

Dissertação para obtenção do Grau de Mestre em
Engenharia de Micro e Nanotecnologias

Supervisor Dr. César António Tonicha Laia, Professor Auxiliar, FCT-UNL

Co-Supervisor Dr. Manuel João de Moura Dias Mendes, Professor Auxiliar convidado, FCT-UNL

Presidente: Dr. Hugo Manuel Brito Águas

Arguente: Dra. Shrabani Panigrahi

Vogal: Dr. César António Tonicha Laia

FACULDADE DE CIÊNCIAS E TECNOLOGIA
UNIVERSIDADE NOVA DE LISBOA

Novembro, 2018

Synthesis of inorganic halide perovskites quantum dots for photoluminescence applications

"Nothing in life is to be feared, it is only to be understood. Now is the time to understand, so that we may fear less."

Marie Curie

Acknowledgments

Primeiramente gostaria de agradecer ao Prof. Rodrigo Martins e a Prof. Elvira Fortunato pelo esforço que dedicaram e continuam a dedicar na criação e continuação deste curso e por proporcionarem oportunidades únicas e inovadoras a todos os alunos que por aqui passaram, e certamente aos que ainda estão por vir.

Importante agradecer ao projecto PTDC/QEQ-QIN/3007/2014. Quero também agradecer ao meu Orientador, Prof. César Laia, e Co-orientador, Prof. Manuel Mendes, pela oportunidade que me deram, por permitirem-me trabalhar numa área nova e pelos conselhos dados ao longo desta experiência. Também necessário um grande agradeciamento à Dra. Sandra Gago que me acompanhou durante todo o percurso, sempre com muita paciência, e que foi indispensável. Ao Tiago Moreira por estar constantemente a emprestar-me células de quartzo. À Andreia Forte pelo apoio no laboratório. E aos restantes membros de laboratório por toda a ajuda disponibilizada.

Obrigada a todos os amigos que tornaram estes 5 anos inesquecíveis. Rita Fragoso por desde o primeiro ano estar presente em todos os momentos importantes. Ao Teles, que apesar de irritar-me profundamente, está sempre disposto a ajudar. Miguel e Fábio por todas os dias passados na 202, almoços durante a tese e fins de tarde na Teresa. Ao Nuno Lima por ser sempre adorável. João Pina e Miguel Ramos, que apesar de terem fugido para a Suécia, também fizeram parte de inúmeras horas na Teresa, conversas e parvoíces. À minha afilhada não oficial "Péssima" Ana Pinheiro pelas risadas, porque só nós percebemos quão brilhantes são as nossas ideias e pelo apoio constante durante estes 4 anos. À Catarina Marques por aturar todas as maluquices dos acima mensionados, inclusive as minhas. À minha colega de materiais, Carolina Pires, pela constante ajuda e por estar sempre pronta com uma palavra amiga. À Carolina Natal por ter tido a vontade de aprender a fazer QDs e por ser uma companhia indispensável no laboratório. Aos restantes, que embora não mencionados, foram muito importantes, obrigada por tudo.

Tenho de agradecer a minha mãe, Rosa, por me aturar, com muita paciência, há 23 anos e por todo o apoio e ajuda nas horas mais difíceis. Ao meu pai, Henrique, que apesar de longe está sempre pronto para me dar conselhos. Aos meus primos por terem sido como irmãos durante a minha infância. Aos meus avós e tia-avó pelo apoio incondicional e por terem sido sempre os meus segundos pais. Em memória ao meu Tio, por me ensinar a importância de um bom livro.

Finalmente, ao meu namorado de há quase 7 anos, Manuel, obrigada por todo o apoio, paciência e dedicação, por ter estado presente em todos os momentos.

Abstract

Metal halide perovskite crystal structures have emerged as an attractive class of optoelectronic materials due to their excellent optical absorption and emission properties. Restricting the physical dimension of the crystallite to the nanometer scale revealed quantum-confinement effects similar to those presented by traditional chalcogenide quantum dots. The synthetized inorganic perovskite quantum dots (IPQD) were characterized by spectroscopic measurements (absorption and photoluminescence emission spectra). Two synthesis methods were studied (supersaturation recrystallization (SR) and hot-injection method (HI)) and the latter was chosen to be employed for the remaining work stages, due to observed better properties. The final goal was to obtain IPQDs doped with metals, focusing in Cd^{2+}. The obtained samples of bromide-based perovskite doped with CdI_2 exhibit more defined emission peaks with smaller full width at medium height (FWHM) and the samples appear to show improved stability when compared with blank $CsPbBr_3$. The smaller FWHM was also observed for the $CsPbI_3$ doped with CdI_2. Inductively coupled plasma atomic emission spectroscopy (ICP-AES) was performed for samples with 10 mol% and 30 mol% of CdI_2, where it was verified that 2.6 % and 8.23 % of the doping was introduced in the final compound, respectively. Note that the latter value was significantly better than those reported in literature (about 2% of the initial amount). The observed optical properties and empirically improved stability make these nanocrystals promising materials in several optoelectronic applications, namely LEDs, solar cells, lasers, among others.

Keywords: inorganic perovskite; quantum dots; nanocrystals; photoluminescence; optical properties; stability; doping

Resumo

Estruturas cristalinas de perovskite à base de metais e halogenetos emergiram como uma importante classe the materiais optoelectronicos, devido às suas excelentes propriedades ópticas. Restringir o tamanho do cristal para a escala nanométrica revelou propriedades de confinamento quântico semelhantes às observadas nos *quantum dots* tradicionais. Os quantum dots the perovskite inorgânicos (IPQD) obtidos foram caracterizados por medidas espectroscópicas (espectros de absorção e emissão). Primeiramente foram analisados dois métodos de síntese (recristalização por supersaturação (SR) e *hot-injection* (HI)). O método de HI foi escolhido para as restantes etapas do trabalho. O objectivo final é o de obter IPQD dopados com diferentes metais, tendo como principal foco o Cd^{2+}. As amostras à base de brometo dopadas com CdI_2 apresentam picos de emissão mais definidos e com FWHM menores, para além disso, também aparentam ter maior estabilidade quando comparadas com as amostras de $CsPbBr_3$. Menores FWHM são também observados para as amostras de $CsPbI_3$ dopadas com CdI_2. Análise por ICP-AES foi realizada para amostras dopadas com 10 mol% e 30 mol% de CdI_2, sendo verificado que 2.6 % e 8.23 % da quantidade originalmente colocada encontrava-se presente no composto final, respectivamente. Note-se que o último valor é significativamente melhor do que os reportados na literatura (cerca de 2% da quantidade inicial). Estas propridades combinadas com melhor estabilidade, observada empiricamente, tornam estes materiais promissores para diversas aplicações na área da optoelectronica, nomeadamente, LEDs, células fotovoltaicas, lasers, entre outros.

Palavras-chave: perovskites inorgânicas; *quantum dots*; nanocristais; fotoluminescência; propriedades ópticas; estabilidade; dopagem

Abbreviations and Symbols

α	- Absorbance coefficient
λ	- Wavelength
λ_{exc}	- Excitation wavelength
ν	- Frequency
A	- Absorbance
a_B	- Bohr radius
A_R	- Reference absorbance
A_S	- Sample absorbance
C	- normalization constant
CB	- Conduction band
d	- Thickness
DMF	- Dimethylformamide
E_g	- Bandgap energy
FA	- Formamidinium
FWHM	- Full width at half maximum
h	- Planck constant
HI	- Hot-injection
ICP-AES	- Inductively coupled plasma atomic emission spectroscopy
IHP	- Inorganic halide perovskite
IPQD	- Inorganic perovskite quantum dot
I_R	- Reference integrated fluorescence intensity
I_S	- Sample integrated fluorescence intensity
LARP	- Ligand-assisted reprecipitation
LED	- Light-emitting diode
LHP	- Lead halide perovskite

MA - Methylammonium

MHP - Metal halide perovskite

NC - Nanocrystal

OA - Oleic acid

OAm - Oleylamine

OD - Optical density

ODE - Octadecene

OIHP - Organic-inorganic halide perovskite

PL - Photoluminescence

PLQY - Photoluminescence quantum yield

QD - Quantum dot

QY_R - Reference quantum yield

SEM - Scanning electron microscopy

SR - Supersaturated recrystallization

TEM - Transmission electron microscopy

VB - Valence band

XDR - X-ray diffraction

Contents

List of Figures

List of Tables

1. Introduction

In the past few years, metal halide perovskites (MHP) have emerged as a major player in the fields of semiconductor and optoelectronics materials, being excellent candidates for several devices, such as photovoltaics, light-emitting diodes (LEDs), lasers and others [1]–[4]. These first attracted interest when Miyasaka's *et al.* reported, for the first time the use of organic-inorganic halide perovskites (OIHP) in a dye-sensitized solar cell, reaching a power conversion efficiency of 3.8% [5]. Recently, a power conversion efficiency of 22.7% was reached for a halide perovskite based solar cell [4], [6].

As with most relevant semiconductor materials, the prospects of their performance when at a nanoscale level are promising. With this premise in mind, in 2014, Julia et al first reported a synthesis of OIHP nanocrystals, revealing 6 nm particles with interesting properties, such as narrow emission band width, varying between 21 to 26 nm, and photoluminescence quantum yields (PLQY) of ca. 20% [6], [7]. Nonetheless, there is no rose without a thorn, and OIHP materials face several hinderances, both in bulk and nanocrystalline formats. Accounted in these are extreme sensibility to moisture, oxygen and heat, which limit the possibility of real-world applications. These limitations have been found to be mostly related to the existence of the organic cation [8].

To tackle the OIHP shortcomings, a logical step was seen in the replacement of the organic cation with less volatile compounds, such as cesium [9], [10]. In 2015, Kovalenko *et al.* reported pioneering work on all-inorganic cesium lead halide perovskites light-emitting nanocrystals [10].

This work strives to synthesize all-inorganic perovskite quantum dots (IPQD) by adapting already existent synthesis methods. A study on metal doping of these IQPDs is also performed, with intent of improving or modifying their properties. These present promising characteristics that make them desirable in different optoelectronic applications.

1.1. Perovskites: General structure and Metal Halide based

Perovskite structure was first observed in the mineral calcium titanate ($CaTiO_3$) and was then defined as a class of crystalline compounds that adopt the ABX_3 structure, where A and B are cations of several valences and ionic radii and X is an anion [11], [12]. The most known perovskites are oxide-based and have been intensively researched due to their ferroelectric, magnetic and superconductive properties [13].

Nevertheless, this work will focus on MHP, more precisely lead halide perovskites (LHP),where A is a monovalent organic or inorganic cation [typically methylammonium (MA),

$CH_3NH_3^+$, formamidinium (FA), $HC(NH_2)_2^+$ or, for the inorganic cation, Cs^+], B represents a bivalent cation (typically Pb^{2+}) and X corresponds to a halide anion (Cl^-, Br^-, I^- or their mixture) that is bound to both cations [11], [12], [14], [15]. As can be observed, A, B and X sites can be occupied by various elements providing a good compositional flexibility that allows the fine tuning and optimization of the optical properties to the desired characteristic for each application [4], [6], [15]. The general formula of the MHP and different compositional elements is represented in Figure 1.1. This class of materials can be divided into two different families according to the nature of the 'A' cation: OIHP (organic cation) and all-inorganic halide perovskites (IHP), the latter being the prime focus of this work.

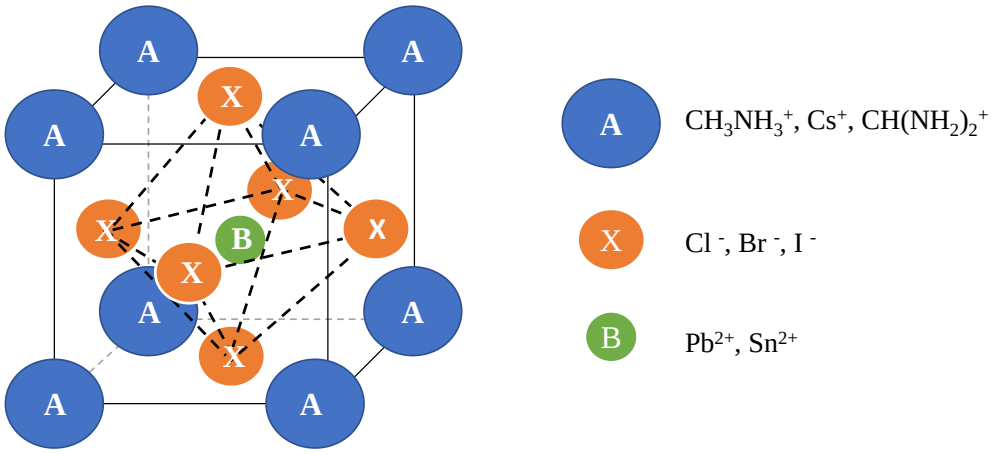

Figure 1.1 Perovskite general formula for MHP and different possible compositions.

MHP were first observed in cesium lead halides ($CsPbX_3$) by Moller, in 1958 [3], [11]. These materials showed photoconductivity properties that could be tuned by varying the halide [3], [11], [16]. Later, in 1978, Weber observed, for the first time in perovskites, the organic cation MA [3], [11], [17]. The OIHP family was the first to attract researches attention, namely the $MAPbX_3$, due to their tunable band gap, possibility of low-cost solution-based processes, long diffusion length, large absorption coefficients and high charge carrier mobility [1], [18]. However, these materials are extremely sensitive to moisture, heat and oxygen. In some of the proposed degradation mechanisms the main problem is the deprotonation of the MA^+, forming a highly volatile compound, CH_3NH_2 [8], [19]. These limitations pose a problem for fabrication, storage and device operation [8].

1.2. Low-dimensional materials

Low-dimensional materials correspond to particles with at least one dimension in the nanoscale range (1-100 nm) and have been increasingly attracting interest due to their unique optical properties that are not present in the bulk material [4]. These materials can present different

morphologies, namely 2D nanostructures (nanoplates and layered structures), 1D nanostructures (nanowires and nanorods) and 0D nanostructures (quantum dots or nanocrystals) [2], [12], [19]. Therefore, the optical properties are strongly influenced by nanomaterial shape and size [2], [20], [21].

Recently, a new type of LHP materials appeared, colloidally synthesized nanometer-scale crystals, that immediately attracted interesse and present promising applications [4], [22]. This type of materials allow bandgap (colour) tunability through the tailoring of the chemical composition (this property is also present in the bulk material) and through quantum confinement – nanostructuring [12]. This work will focus in low-dimensional all-inorganic perovskite nanocrystals or quantum dots.

1.2.1. Quantum dots – Quantum confinement effect

Quantum dots (QD) were first observed, by Mark Reed *et al.* , in a GaAs nanostructure by means of scanning electron microscopy (SEM) [23]. Nowadays, QD are described as zero-dimensional semiconductor particles that exhibit unique electrical and optical properties when compared with their bulk counterparts [24].

The electronic structure of bulk semiconductors is arranged in two bands: the valence band (VB) and the conduction band (CB). The CB corresponds to the overlap of the unoccupied energy levels and the VB corresponds to the occupied levels. These two bands are separated by an intra-band energy spacing – band gap. When light excitation occurs, and electron-hole pair is formed, and the semiconductor becomes conductive, the energy required for this to take place should be larger or equal than the bandgap energy (E_g) [20]. Restricting the size to the nanometer scale causes the transition from continuous to discrete energy levels, leading to a shift towards a higher energy as the nanoparticle size reduces [20]. The absorption and emission properties became size dependent [25]. This is known as quantum confinement effect. The degree of confinement is related with the Bohr radius (a_B) of the material. A strong confinement occurs when the radius of the nanomaterial is lower than three times the Bohr radius. In contrast, a weak confinement happens when the radius is between three to ten times the Bohr radius [8], [20]. Quantum confinement effect schematic is presented in Figure 1.2.

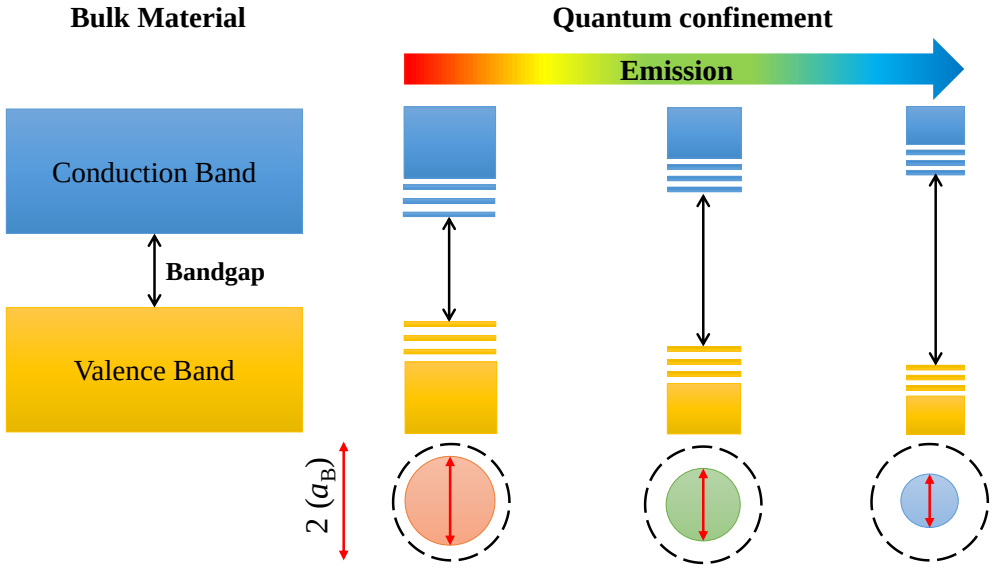

Figure 1.2 Schematic of the quantum confinement effect. Bulk material continuous energy levels versus nanomaterials discrete energy levels and representation of different degrees of confinement.

1.3. All-inorganic halide perovskite quantum dots

As previously mentioned, LHP allow bandgap compositional engineering. In parallel, these properties can also be altered by reduction of the crystal size – low-dimension strategy – taking advantage of the quantum confinement effects above referred [11].

Motivated by the success of the OIHP, Kovalenko *et al.* reported a synthesis of all-inorganic perovskite quantum dots (IPQD) with the chemical formula of $CsPbX_3$ (X = Cl, Br, I or mixed halide systems) [10]. The obtained QDs exhibited remarkable optical properties and size-dependent bandgap across the entire visible spectra, with high PLQYs of 50-90 %, narrow emission band width of 12-42 nm and radiative lifetimes between 1-29 ns (faster emission for QDs with wider bandgap) [10]. IPQDs combine the advantages of perovskites with the aforementioned quantum confinement effects [9], [19]. Simultaneously, these systems present better stability than the OIHP, as verified by Zeng *et al.* , through comparison between the PLQYs of $CsPbX_3$ and $(CH_3NH_3)PbBr_3$ nanocrystals during storage [2], [21]. Shortly after their report, a wide number of studies have been carried out making these family of nanocrystals an important and rapidly developing subfield [15], [21]

1.3.1. Synthesis methods for colloidal nanocrystals

Colloidal LHP nanocrystals have been investigated for several applications and various approaches have been proposed. However, the most common are the hot-injection method (HI) –

synthesis of IHP - and the ligand-assisted reprecipitation (LARP) method - synthesis of OIHP [26].

The hot-injection method for the synthesis of IPQDs was proposed by Kovalenko *et al.* in 2015 [10]. The HI method was first proposed by Murray *et al.* , in 1993, for the synthesis of cadmium chalcogenides QDs (to date is the main method for producing these QDs) [27], [28]. This method can also be employed for the synthesis of 2D nanostructures – nanoplates and nanowires [8]. A drawback in the HI method is the necessity of high temperatures and controlled atmosphere.

In 2016, Zeng *et al.* reported an IPQD synthesis at room temperature and free from the inert gas [29]. This system presented PLQY between 10 to 95 % and FWHM of 12-35 nm [29]. This method is based on supersaturation recrystallization (SR) and it is inspired by the LARP method, utilized in the synthesis of OIHP nanocrystals [26], [30].

These methods will be further described in the Results and Discussion section.

1.3.2. **Doping of IPQDs**

As previously mentioned, perovskites present good composition flexibility. This concept can be applied to IPQD by doping them with other elements (Sn^{2+}, Mn^{2+}, Zn^{2+} and Cd^{2+}) in order to replace one part of the perovskite (normally Pb^{2+}) to modify the optoelectronic properties [6].

In 2016, Jellicoe *et al.* reported a lead-free halide perovskite QD through replacing lead with tin, achieving $CsSnX_3$ [31]. However, the obtained QD were unstable under ambient conditions due to the chemical instability of the element in the required oxidation state (Sn^{2+}). This system presented significantly lower performances when compared with lead-containing perovskites – PLQY of 0.14 % and lifetimes around 0.7 to 8 ns [31], [32]. Instead of complete substitution of the lead component, Li *et al.* indicated that Mn^{2+} could act as dopant in perovskite nanocrystals by adding a Mn source to a typical high-temperature synthesis method (HI) [33]. This approach only worked for $CsPbCl_3$ nanocrystals. Doping Mn^{2+} into $CsPbBr_3$ and $CsPbI_3$ can be achieved by post-synthesis cation exchange. Sam *et al.* demonstrated that this tactic can be used for doping the perovskite with other elements – Pb^{2+} can be partially substituted by several cations, such as, Sn^{2+}, Cd^{2+} and Zn^{2+} [6], [34].

2. Materials and Methods

2.1. Synthesis methods

In this study, $CsPbX_3$ quantum dots were synthesized according to a modified colloidal synthetic approach previously reported, being used two different synthesis: hot-injection method and supersaturation recrystallization method [10], [29], [35]. The reagents in both methods were employed as received without further purification. The chemicals used were purchased from different distributers: from Aldrich were Cs_2CO_3 (99%), oleic acid (90%), octadecene (90%), PbI_2 (99.999%) and CsI (99.9%); from Acros Organics oleylamine (80-90%); from Alfa Aesar $PbBr_2$ (99.999%) and CsI (99.99%).

The nanoparticles were doped with different transition metals, also used without further purification, namely, Cd(II), Zn(II) and Cu(I). The chemicals used for doping the QDs were purchased from different distributers: from Riedel $ZnCl_2$ (98%); from Sigma-Aldrich CuBr (98%); from Aldrich CdI_2 (99%).

2.1.1. Hot-injection method

Cs-oleate preparation: The Cs-oleate was prepared as described by Chen *et al.* [35]. A mixture of Cs_2CO_3 (1.23 mmol) and CuBr at a designated Cu/Cs mole ratio between 0 and 10 mol% was loaded into a 100 mL 2-neck flask containing oleic acid (1.5 mL, OA) and octadecene (15 mL, ODE) and degassed under N_2 flow at room temperature for 20 min. It was then heated to 150 ºC, under vigorous stirring, until complete dissolution of Cs_2CO_3, maintaining the N_2 flow. After cooling to room temperature, the precursor solution was kept under N_2 atmosphere. Given that the Cs-oleate precipitates out of ODE at room-temperature, the solution must be heated to 110 ºC before injection.

Synthesis and Isolation of the prepared QDs: As previously mentioned, the QDs were synthesized according to a modified approach reported by Chen *et al.* [35]. A mixture of PbX_2 (0.188 mmol) such as PbI_2 (0.087 g) and $PbBr_2$ (0.069 g) and AX_2 (A = Zn(II), Cd(II); X = Br, I, Cl) at a designated dopant/Pb mole ratio between 0 and 50 mol% was added to a two-neck flask containing ODE (5 mL), OA (0.5 mL) oleylamine (0.5 mL, OAm). The mixture was degassed under N_2 flow at room temperature for 20 min and then heated to 120 ºC, maintaining the N_2 flow, with constant stirring for 60 min to remove the moisture of the raw components. Thereafter, the solution was heated to 150 ºC under N_2 and constant stirring, followed by a rapid injection of 0.4 mL of the Cs-oleate precursor and, 5 to 10 s later, the final solution was cooled by an ice-water bath.

The obtained QDs were collected by centrifugation at 5000 rpm for 20 min and then redispersed in hexane for a long-time stable solution.

2.1.2. Supersaturation recrystallization method

This method only allowed the synthesis of $CsPbBr_3$ and follows the method previously described by Zeng *et al.* [29].

Precursor solution synthesis: A mixture of 0.4 mmol of CsBr and $PbBr_2$ is added to a beaker containing 10 mL of dimethylformamide (DMF), 1 mL of OA and 0.5 mL of OAm. The mixture remains under stirring until the CsBr and $PbBr_2$ are fully dissolved.

Synthesis and isolation of $CsPbBr_3$ QDs: In a beaker containing 10 mL of toluene under vigorous stirring is quickly added 1 mL of the precursor solution above described. The mixture remains under vigorous stirring for a about 1 min to allow more formation of nanoparticles. The obtained QDs were collected by centrifugation at 5000 rpm for 20 min and then redispersed in hexane for a long-time stable solution.

2.2. Characterization

2.2.1. Absorption and Emission profiles

Absorption spectra: Taken in a quartz cell with a 1 cm optical path. The absorption spectra was measured in a spectrophotometer, from 200 to 800 nm, Cary 100, and the baseline was performed with both sample and reference compartments empty. All spectra measurements were done at room temperature.

Emission spectra: Taken in a quartz cell with 1 cm optical path and clear sides. Measured in a HORIBA spectrofluorometer model iHR 320, with a slit of 1 nm. All spectra measurements were performed at room temperature. PLQYs were estimated according to standard procedure using appropriate dye molecules for green and red (coumarin 343 and rhodamine 6G, respectively).

2.2.2. Inductively coupled plasma atomic emission spectroscopy

The metal content was determined by inductively coupled plasma atomic emission spectroscopy (ICP-AES), carried out on a HORIBA Jobin Yvon ULTIMA sequential ICP. A monochromator with a Czerny Turner spectrometer was used. The utilized gas was Argon. The chosen wavelengths and experimental conditions are summarized in Annex A.

3. Results and Discussion

Perovskite semiconductor materials, like the IPQDs presented here, are as interesting as they are complex, exhibiting interesting optoelectronic properties. In this work, the optical characteristics of this class of materials are explored via spectroscopic measurements, namely absorption and photoluminescence emission spectra.

As a starting point, two synthesis approaches were compared, and one was chosen and employed for the remain of the work. Different metals were incorporated into the synthesis, with the intent of acting as dopants in the crystal structure, altering the optical properties of the base $CsPbBr_3$ QDs. The choice of the halide (bromide) was influenced by the stability properties reported in literature.

Cadmium was chosen for further investigation due to its ionic radius being closer to the one presented by Pb^{2+}. This, theoretically, should lead to lessened deformation of the crystalline lattice. Finally, to better understand the influence of Cd a sample of $CsPbI_3$ and of Cd-doped $CsPbI_3$ were characterized.

It is important to mention that, for an accurate characterization of these materials, further techniques should be employed, such as X-ray diffraction (XDR), transmission electron microscopy (TEM), time-resolved photoluminescence (PL) decays, among others. For simplicity sake and due to time constraints, only spectroscopic measurements and ICP-AES analyses were performed. As these are novel materials, there is a rather steep learning curve when it comes to the synthesis and studying of their properties as there are several nuances in the synthesis process, purification, stability and manipulation of these materials.

3.1. Synthesis Methods: Supersaturation Recrystallization and Hot Injections

Bulk metal halide perovskites, $CsPbX_3$ can be traced back to 1950s. However, at the time these failed to attract interest due to their poor optical properties and difficult fabrication. Only since 2015, with the cesium-lead halide perovskite high-quality colloidal nanocrystals, synthetized by the hot-injection method reported by Kovalenko *et al.* , that this type of material has been intensively explored in a variety of directions [10], [16]. Kovalenko's method followed an adaptation of the already existing and commonly used HI procedure for the synthesis of metal chalcogenide or fluoride QDs. This method has been employed by several groups to obtain colloidal low-dimensional IP with different halide compositions, shapes and sizes. [15], [21]. This synthesis procedure takes advantage of the ionic nature of the chemical bond in the $CsPbX_3$ compounds.

Controlled precipitation of Cs^{+}, Pb^{+2} and X^{-} ions into $CsPbX_3$ is achieved by the injection of cesium oleate into a high temperature – 140 to 200 ºC – octadecene (high boiling point solvent) solution containing PbX_2 and organic ligands. Long-chain organic ligands confine the crystal size, different ratios of the same ligands or utilization of different chain size ligands will lead to different morphologies – for QDs the employed long-chain ligands are OA and OAm with an equal molar amount [21]. The crystal growth occurs manly in the first 3 seconds after the injection process due to a fast nucleation and growth kinetics [4]. Therefore, the QDs crystal size can be precisely tuned by changing the synthesis temperature rather than by the reaction time [10]. Higher temperatures lead to larger nanoparticles. By altering the reaction time, the long-chain ligands or the ratio of OA to OAm in the hot injection system, while maintaining the remaining conditions, the morphology can also be tuned [15]. This method cannot be applied to OIHP nanocrystals due to low stability of the organic cation at higher temperatures.

In 2015, Zhang *et al.* reported the LARP method for synthesis of $MAPbX_3$ (X = Cl, Br, I). This method was based on the reprecipitation of PbX_2 and the organic halide salt (CH_3NH_3X) in the presence of ligands. These are dissolved in strongly polar solvents and are subsequently added to a solution containing a non-polar medium, also in the presence of ligands. The abrupt difference in solubility triggers the recrystallization of lead halide perovskite nanocrystals [26], [36].

Zeng *et al.* reported the synthesis of IPQDs under room temperature and without atmosphere control inspired by the LARP method – supersaturation induced recrystallization (SR). Similarly to the above described method, the significant differences in solubilities for Cs^{+} and Pb^{2+} in DMF (polar solvent) and toluene (non-polar solvent) lead to, as the transfer from DMF to toluene occurs, a rapid formation of a highly supersaturated state that induces the rapid recrystallization in the form of $CsPbX_3$ nanocrystals. Without the presence of long-chain organic ligands this synthesis cannot take place, as these confine the crystal size and act as surface ligands (colloidally stabilize the obtained nanostructure). In the SR process the reaction is very rapid making the kinetic control of the nanocrystals growth difficult – as such the shape and size of the obtained QDs is instead done via alteration of the ligands utilized during synthesis [8], [15], [18], [21], [26]. This method presents a significant disadvantage as the presence of polar solvent can induce a more rapid degradation of the nanocrystals – as perovskite materials are extremely sensitive to polar mediums.

Both methods resulted in well-defined peaks with small full width at half maximum (FWHM), as seen in Figure 3.1. The obtained photoluminescence emission spectra allow to infer that perovskite QDs were synthetized, as they are consistent with those seen in literature [10], [29], [35]. For the HI synthesis, as previously mentioned, a change in temperature leads to a

variation in the QDs crystal size and thus a temperature of 150 ºC was set for the entirety of the work, so as not to introduce any further variables in the synthesis. The nanocrystals (NCs) synthetized through the SR method were notoriously cloudier and not as bright when compared with the HI samples. These observations, for both cases, were consistent with the findings in literature.

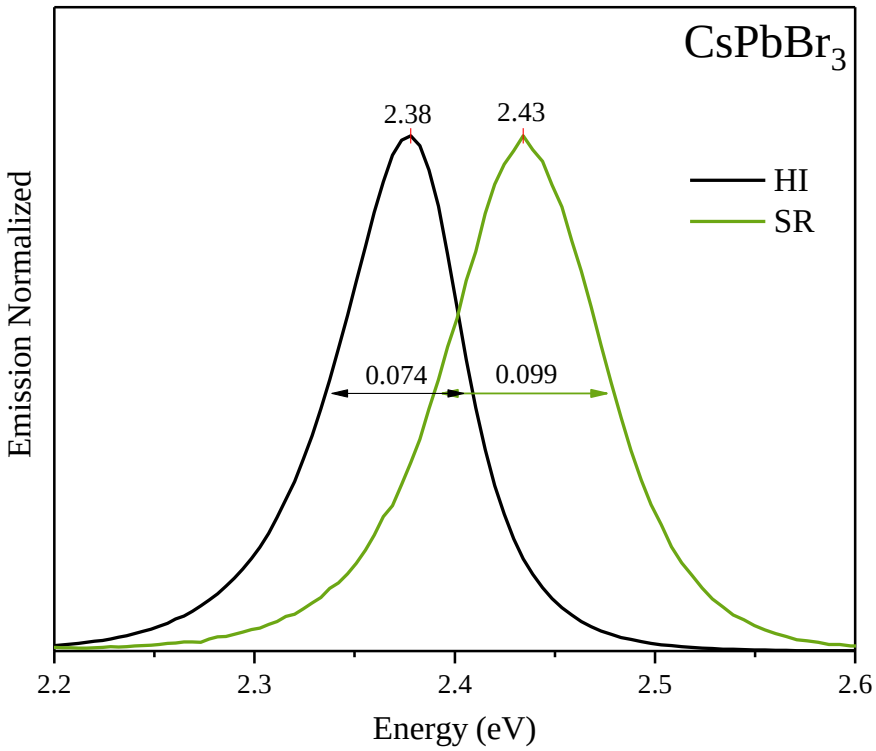

Figure 3.1 Normalized photoluminescence emission spectra with an excitation wavelength (λ_{exc}) of 450 nm for $CsPbBr_3$ obtained via SR (green line) and HI (black line) synthesis method.

It is important to mention that, contrary to what is described in previous works, the synthesis of $CsPbI_3$ was not successful with the SR method. To obtain a positive result, an increase of the amount of OAm and controlled N_2 atmosphere was necessary. Luminescence was only present for a brief period (few minutes), after which the solution took on a yellowish colour and precipitated. This is thought as being related to an undesired transition from the cubic phase (α-$CsPbI_3$) to an insulating phase – orthorhombic (δ-$CsPbI_3$) - at room temperature, the cubic phase is only thermodynamic preferred for temperatures above 315 ºC [8], [16], [37]. The synthesis of $CsPbI_3$ via HI method was successful and the obtained photoluminescence spectra is in accordance with literature and is presented in Figure 3.2 [10]. However, when compared with $CsPbBr_3$ QDs, stability in a non-controlled environment is visibly inferior – the bromide-based QDs maintained their fluorescence for several weeks after the iodide-based ones lost theirs.

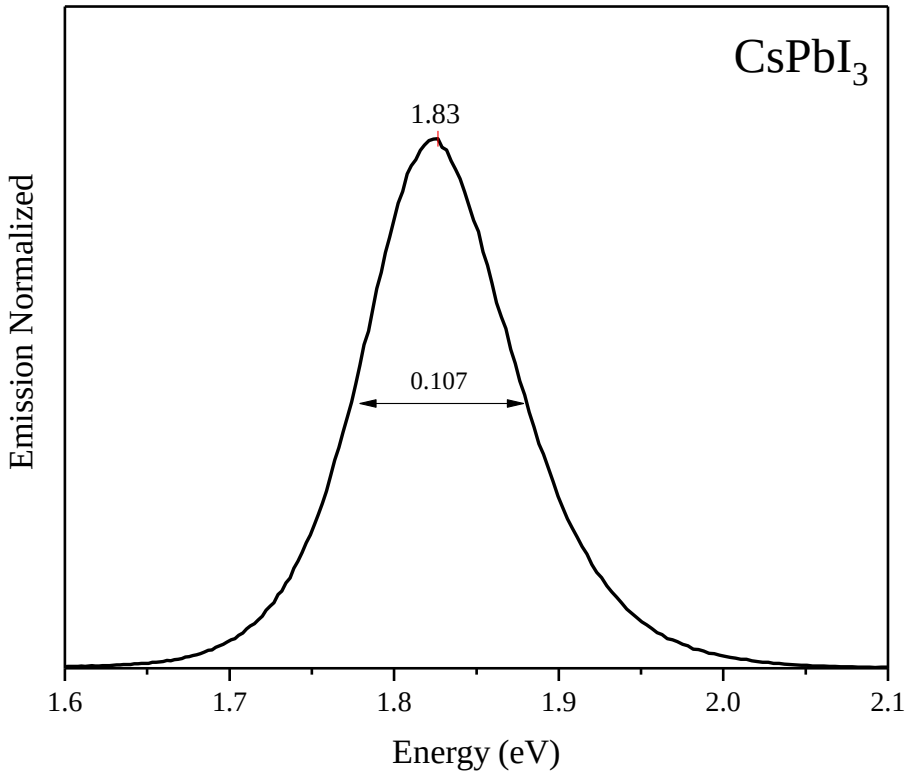

Figure 3.2 Normalized photoluminescence emission spectra (λ_{exc} = 450 nm) for $CsPbI_3$ sample produced by HI method.

The obtained emission peaks and FWHM of the three samples ($CsPbBr_3$ via SR and HI method and $CsPbI_3$ by HI method) are presented in Table 3.1. Taking the previous observations in consideration, and the fact that the FWHM was 25 % smaller for the HI method when compared with the SR synthesis, the former was chosen and employed for the remaining of the work.

Table 3.1 Summary table with the obtained emission peaks and FWHM for the samples produced by SR and by HI method.

	$CsPbBr_3$ (SR)	**$CsPbBr_3$ (HI)**	**$CsPbI_3$ (HI)**
Emission Peak (eV)	2.43	2.38	1.83
FWHM (eV)	0.099	0.074	0.107

3.2. Doping of $CsPbBr_3$ with different elements.

In contrast to traditional QDs, the crystal size presents a lower impact in the bandgap tuning. The main factor in controlling the nanocrystal emission is, in fact, the composition of the crystal itself. Composition control can be achieved by modifying the halide or using a mixture of halides, Cl/Br and Br/I - Cl/I mixture is not possible due to the large difference in the ionic radii of the Cl^- and I^- ions [18]. Moreover, metal doping (such as Mn^{2+}, Sn^{2+}, Cd^{2+} or Zn^{2+}) can also be employed as an alternative route to manipulate the optoelectronic properties of the IPQDs – attained by replacing one of the elements in the original structure [6], [12], [18]. Doping with these metals has been previously done, but only through cation exchange mechanisms (post-synthesis) [6].

It is important to notice that, even though three metals were studied (Zn^{2+}, Cu^+ and Cd^{2+}), the available reagents were not ideal. Preferably the employed metal halides should present the same halogen as the intended perovskite structure, but this was only possible for the bromide-based samples doped with Cu^+ (CuBr) and for the iodide-based samples doped with Cd^{2+} (CdI_2). Bromide-based IPQDs were doped with CuBr, CdI_2 and $ZnCl_2$ and the iodide-bases IPQDs were only doped with CdI_2. The obtained photoluminescence emission spectra are presented in Figure 3.3.

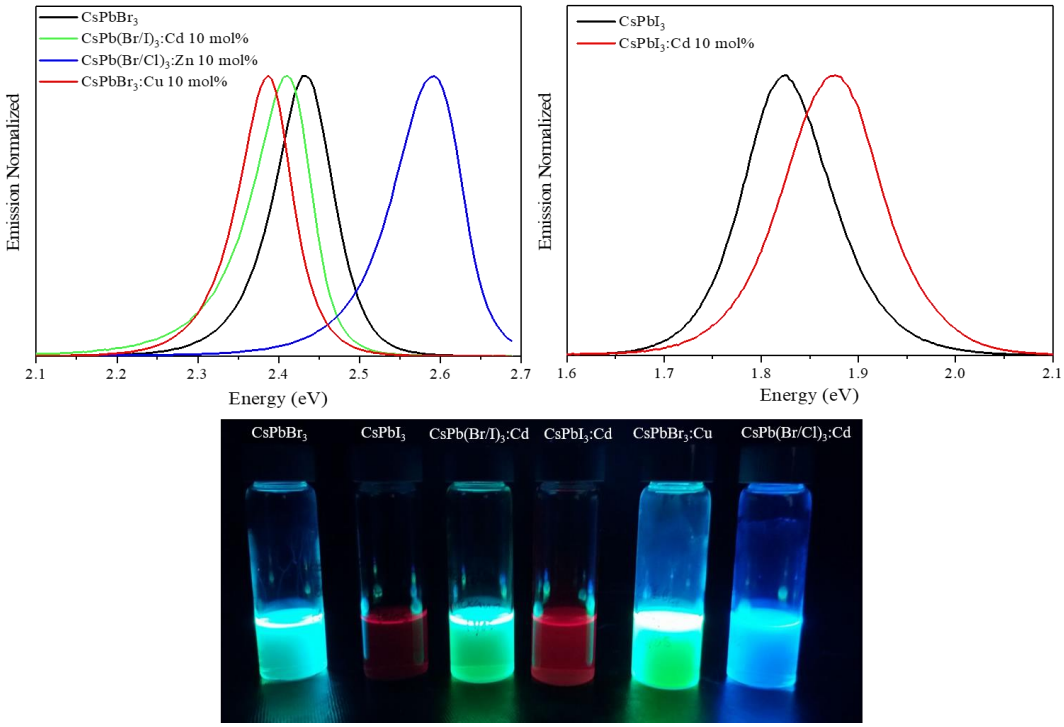

Figure 3.3 Normalized photoluminescence emission spectra (λ_{exc} = 450 nm for all samples). Bromide-based samples on the left and iodide-based samples on the right (above plots). Below are the obtained samples under UV-lamp.

The Cu-doping was performed with the partial replacement of Cs^+ in mind, while the remaining cases had the substitution of the Pb^{2+} as the objective. An expected difficulty arose in the Cu-doping procedure – the facile oxidation in solution of the CuBr when expose to ambient atmosphere made the synthesis and reproduction troublesome. The red- and blue-shifts in the emission spectra with CdI_2 and $ZnCl_2$, respectively, raised the suspicion that these were due to partial replacement of the Br^- with Cl^- (for Zn^{2+}) and I (for Cd^{2+}) due to the fact that, according to literature, IPQDs containing chloride suffer a blue-shift and the ones with iodide suffer a red-shift when compared with $CsPbBr_3$ QDs [10]. A summary of the attained emission peaks and FWHM is presented in Table 3.2. It is observable that the FWHM increases for the iodide-based samples, this was expected and is according to the values present in literature [10]. The absorption properties will be divided into two sections: iodide-based samples and bromide-based samples.

Table 3.2 Summary table of the emission peaks and FWHM of the bromide- and iodide-based samples IPQDs.

Samples	Emission peak (eV)	FWHM (eV)
$CsPbBr_3$	2.43	0.086
$CsPb(Br/Cl)_3$:Zn 10 mol%	2.59	0.099
$CsPb(Br/I)_3$:Cd 10 mol%	2.41	0.087
$CsPbBr_3$:Cu 10 mol%	2.39	0.078
$CsPbI_3$	1.83	0.107
$CsPbI_3$:Cd 10 mol%	1.88	0.119

3.2.1. Iodide-based samples: optical properties

Although the iodide-based QDs exhibited the expected red fluorescence, the samples showed a strong absorption peak at 3.34 eV (370 nm) - same for both samples - that completely masks the smaller one at approximately 2.13 eV (581 nm), shown in Figure 3.4. This was initially thought to be related with an undesired transition from the cubic to orthorhombic phase, and the difference between these should be properly understood. The $APbX_3$ perovskite cubic phase (α-phase) is composed of a 3D corner-sharing metal halide octahedra ($[PbX_6]^{4-}$), while the monovalent cation (A site, in this case Cs^+) occupies the octahedral voids caused by the halogens, balancing the charge and providing geometrical stability. For the $CsPbI_3$ instance, the cubic phase is thermally unstable at room temperature – the increase of the ionic radii leads to the Cs^+ ions being too small

to stabilize the 3D $[PbI_6]^{4-}$ octahedra – transitioning to a polymorph with a lower dimensionality (1D) – orthorhombic phase - and, consequently, a wider bandgap [37], [38]. However, this option was discarded since no absorption features appeared at the 2.81 eV region (440 nm) - which corresponds to the orthorhombic $CsPbI_3$ absorption band-edge [39]. Further research lead to the belief that another undesired polymorph, Cs_4PbI_6 corresponding to a rhombohedral crystal structure is present. In this phase, the $[PbX_6]^{4-}$ octahedra are no longer corner-shared, leading to a much stronger quantum confinement than the one observed in $CsPbI_3$. According to literature, the Cs_4PbI_6 phase presents a strong peak at 3.37 eV (367 nm) with the same profile of the one observed [38], [40]. The 3.34 eV peak has the exact same profile and position for both samples leading to the conclusion that it most likely is the same chemical compound.

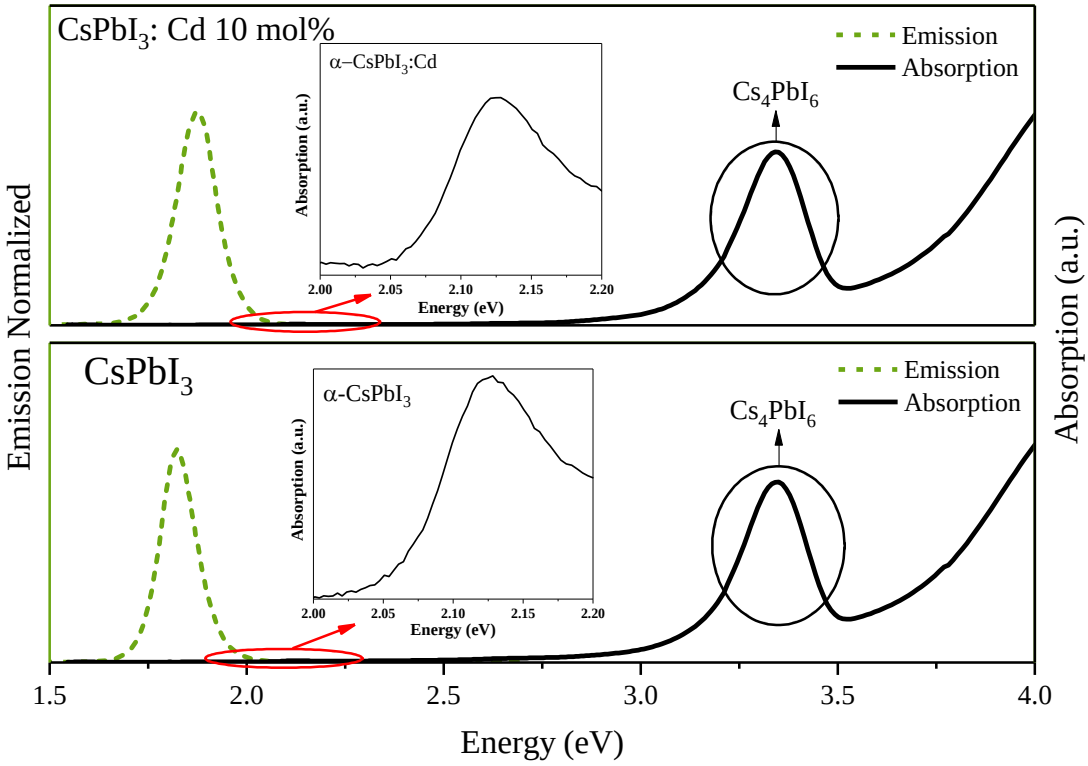

Figure 3.4 Absorption and normalized photoluminescence emission (λ_{exc} = 450 nm) spectra of the iodide-based samples: above $CsPbI_3$: Cd 10 mol% and bellow $CsPbI_3$. Absorption spectra corresponds to the full-line (black) and the emission spectra corresponds to the dash-line (green).

The presence of hybrid nanoparticles of $CsPbBr_3/Cs_4PbBr_6$ has been reported, in which the $CsPbBr_3$-phase is pointed as responsible for the strong green emission. A similar situation might be present in the iodide-based samples as these exhibit the characteristic strong red-emission even though the absorption band that corresponds to the $CsPbI_3$ is not visible when observing the whole spectrum (only observable when zooming in the 1.77 to 2.5 eV range). Nonetheless, is important

to take into consideration that, as previously mentioned, the iodide-based samples are rather unstable, and the obtained results may also be consequence of an already existing degradation of the samples. Therefore, the PLQYs and bandgaps were not calculated for the $CsPbI_3$ region. The bandgap correspondent to the absorption band at 3.34 eV (370 nm) was calculated according to the Tauc relation (will be explained in the next section of the work) – 3.19 eV for both samples.

3.2.2. **Bromide-based samples: optical properties**

Similarly to the iodide-based samples, the absorption profiles were measured and are presented in Figure 3.5, along with the emission profile. For the $CsPbBr_3$ sample, while the emission shows accordance with literature for QDs (nanocubes) the absorbance profile goes against it [10], [41], [42]. Instead, the latter exhibits resemblance to those presented by Alivisatos *et al.* for nanoplates (with 5-unit perovskite cell) [41]. To assure a low enough optical density (OD) for the procedure - absorbance of 0.1 at the excitation wavelength - further dilution of the samples took place and the measurements were not taken immediately after – which may indicate that, as previously observed for OIPH and IPQDs, the formation of nanoplates is being induced by the dilution procedure [42]. The absorbance profile for the doped samples have a closer resemblance to the one seen in $CsPbBr_3$ nanocubes, especially the $CsPbBr_3$:Cu 10 mol% and the $CsPb(Br/I)_3$:Cd 10 mol% . It is notorious that, with the increased dilution, the emission peak suffers a slight blue-shift – for the $CsPbBr_3$ the peak is very similar to the one observed for the nanoplate morphology [41].

The bandgaps were calculated based on the absorbance profiles, following the Tauc approximation under the assumption that IPQDs have low scattering and, therefore can be ignored. The optical bandgap can be estimated following the Tauc relation:

$$(\alpha h\nu)^{1/n} = C(h\nu - E_g) \quad (1)$$

where α is the absorption coefficient, h is the Planck constant, ν is the frequency, C is a normalization constant, E_g is the bandgap and n value is related with the nature of the electronic transition between the valence and conduction band. The absorption coefficient can be calculated according to the relation:

$$\alpha = 2.303\frac{A}{d} \quad (2)$$

where A is the absorbance and d is the thickness (of the utilized cuvette – 10 mm). The $CsPbX_3$ QDs present a direct allowed transition and, hence, the n takes the value 1/2, and the bandgap is calculated through the interception point on abscissa of the $(\alpha h\nu)^{1/n}$ vs $h\nu$ plot [43], [44]. The Tauc plots are presented in Annex B.

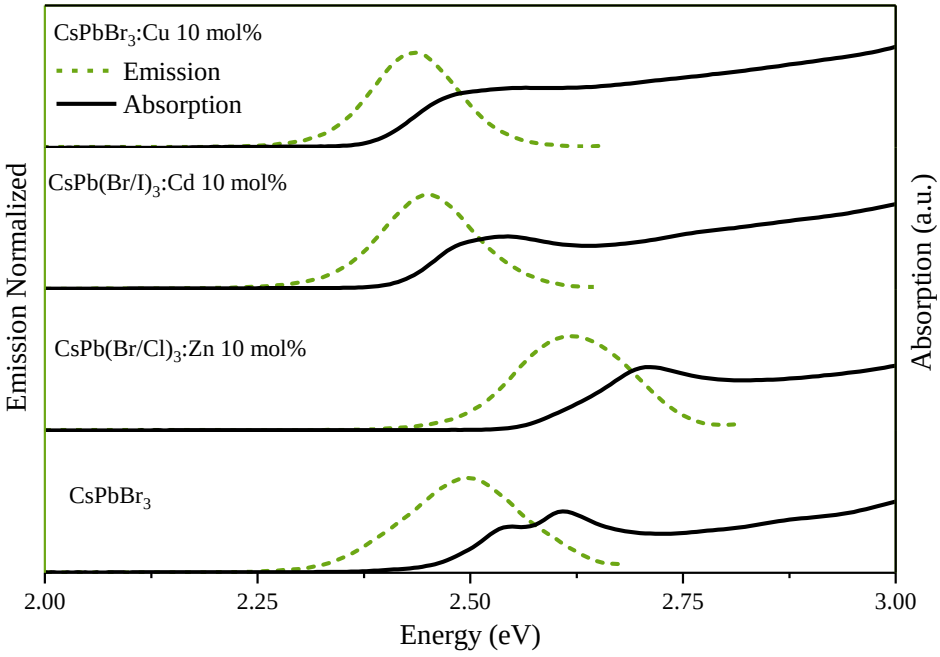

Figure 3.5 Absorption (full-line) and normalized photoluminescence emission (dash-line) spectra for bromide-based samples. Emission spectra λ_{exc} = 450 nm for all samples (except for CsPb(Br/Cl)$_3$:Zn 10 mol%, λ_{exc} = 430 nm).

The PLQYs of the samples were calculated using a comparative method – estimated by a standard procedure using dye molecules (in this case, Coumarine 343 – green emission - and Rhodamine 6G – red emission). In this comparative method, a reference fluorophore is used (i.e. a standard) which possesses known quantum yields and emission and absorbance properties close to that of the sample of interest, under the same excitation conditions (λ_{exc}). Absorbances of all solutions are adjusted to a value of, at maximum, 0.1 at the λ_{exc}. The value is obtained following the equation (3) where QY_R is the reference standard quantum yield, I_R and I_S is the integrated fluorescence intensities (photoluminescence emission spectra area) for the reference and sample, respectively, and A_S and A_R are the absorbance values at λ_{exc} for the sample and reference, correspondingly.

$$PLQY = QY_R \frac{I_S}{I_R} \frac{A_R}{A_S} \times 100 \quad (3)$$

The obtained PLQYs and bandgaps are presented in Table 3.3. The expected bandgap values for $CsPbBr_3$ QDs (nanocubes) with emission peak at approximately 2.42 eV (510 nm) is 2.44 eV and the expected bandgap for $CsPbBr_3$ nanoplates is around 2.52 eV [9], [10]. The bandgap obtained for the $CsPbBr_3$ sample is significantly closer to those expected of a nanoplate (2.49 eV). For the remaining cases, the absorption profiles present more similarities to those commonly observed for nanocubes, which might indicate that the dilution does not affect the sample

morphology. When it comes to the PLQYs, the one described for $CsPbBr_3$ nanoplates is rather sensitive to the thickness – the smaller the thickness the lower the PLQYs – with values varying from 84 to 10 % [41]. For the nanocubes the values are normally higher, varying between 50 to 90% - higher values for the IPQDs with higher ratios of bromide.

Table 3.3 PLQYs for bromide-based samples. Coumarine 343 standard dye.

	$CsPbBr_3$	**$CsPb(Br/I)_3$:Cd 10 mol%**	**$CsPbBr_3$:Cu 10 mol%**	**$CsPb(Br/Cl)_3$:Zn 10 mol%**
PLQYs (%)	34	19	23	17
Bandgap (eV)	2.49	2.44	2.41	2.63

Considering the time-restraints for this work's conclusion, only one of the previous dopants was chosen to further studies. The added difficulty of the Cu-doped IPQDs synthesis and the fact that the ionic radii of Cd^{2+} is closer to the one presented by lead – less possibility of causing stress and deformation of the crystalline lattice - made the Cd-doped ones the best choice to be employed for the remaining work.

3.3. Cd-doped IPQDs

3.3.1. Cd-doping in bromide-based samples: optical properties.

Considering that the doping was made by adding CdI_2 to the synthesis of $CsPbX_3$, it was deemed necessary to verify if the red-shift present in the $CsPb(Br/I)_3$:Cd samples is due to the presence of Cd^{2+} or I^-. For that, a study with different doping concentrations of CdI_2 and PbI_2 was devised and carried out (Figure 3.6).

The obtained photoluminescence emission profiles are presented in Figure 3.6. All samples were diluted so that the PLQYs could be readily calculated. The $CsPbBr_3$ sample shows a larger FWHM and a blue-shift of the emission peak. This observation goes in concordance with the dilution-induced nanoplates formation and with the previously discussed bromide samples. It is visible that the emission peaks are very similar for all samples, leading to the conclusion that the red-shift is most likely due to the presence of iodide. Nevertheless, it is also observable that the samples containing Cd^{2+} present more defined peaks with smaller FWHM (the emission peaks, FWHM, PLQYs and bandgaps are further shown in Table 3.4) – for all samples except the $CsPb(Br/I)_3$:Cd 10 mol% - which might indicate that the presence of Cd^{2+} confers same stability to the nanostructure.

The $CsPb(Br/I)_3$:Cd 10 mol% sample appears to present a significant emitting population in the 2.52 eV region (490 nm) which might be related with the presence of $CsPbBr_3$ nanocubes. A second peak at 2.42 eV (510 nm) region is thought to be the $CsPb(Br/I)_3$:Cd 10 mol% domain. The same occurs for the $CsPb(Br/I)_3$ 10 mol% sample, where the beginning of a band formation (less defined when compared with the previous case) is observable and is believed to be related with a population of $CsPbBr_3$ QDs. For the $CsPb(Br/I)_3$ 50 mol% a wide emission band is observed and can be related to the formation of $CsPbBr_{3-x}I_x$ with different Br/I proportions.

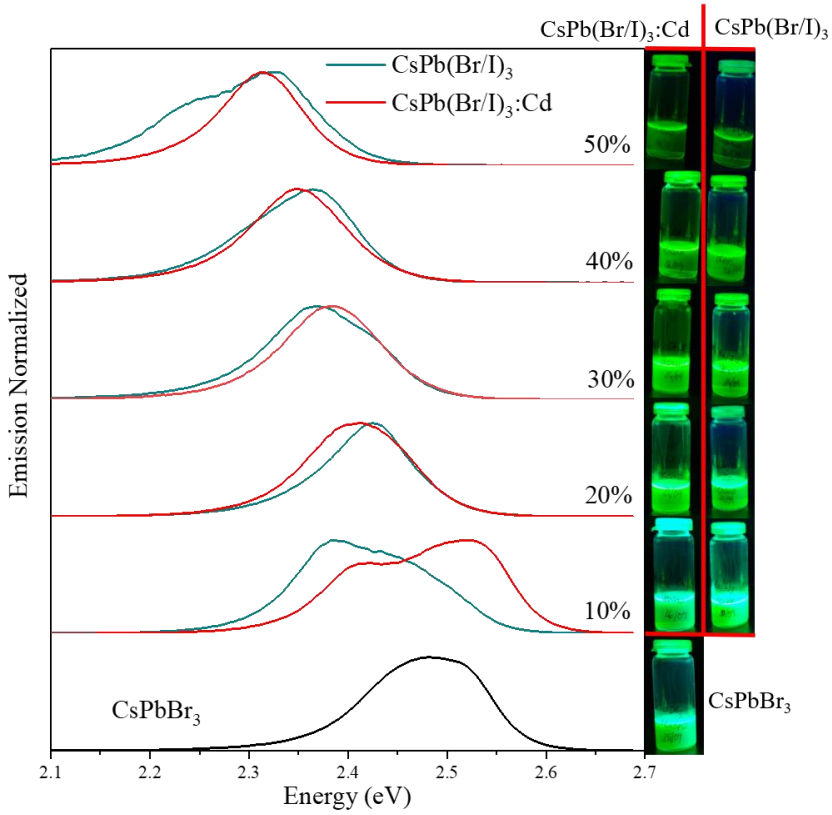

Figure 3.6 On the left, normalized photoluminescence emission spectra (λ_{exc} = 450 nm); $CsPb(Br/I)_3$ with a Br/I ratio of 10, 20, 30, 40 and 50 mol% (blue line) and $CsPb(Br/I)_3$:Cd with 10, 20, 30, 40 and 50 mol% of CdI_2 (red line). On the right, samples under UV-lamp: left are the $CsPb(Br/I)_3$:Cd with 10, 20, 30, 40 and 50 mol% of CdI_2 and right are the $CsPb(Br/I)_3$ with a Br/I ratio of 10, 20, 30, 40 and 50 mol% of PbI_2 (mol% are aligned with the respective emission profiles).

The comparison between emission and absorption profiles are shown in Figure 3.7. It is easily observable that the absorption profiles are rather similar for the same percentages, again indicating that the shift might be related with the presence of iodide – meaning that the presence of Cd^{2+} might not be significantly altering the optical properties. The bandgaps were calculated following the Tauc relation and are shown in Table 3.4. The samples display an absorption band in the 4 to 5 eV region (for all except the $CsPbBr_3$, $CsPb(Br/I)_3$:Cd 50 mol% and the $CsPb(Br/I)_3$

50 mol% samples) with bandgaps varying between 3.7 and 3.89 eV. The obtained bandgaps are close to the one expected of Cs_4PbBr_6 (3.95 eV) [38]. This behavior was previously observed in the iodide-based samples – where both the rhombohedral and cubic phases may be present, being the latter responsible for the bright green emission. The complete absorption profile for the $CsPbBr_3$ sample (where the band at 4 to 5 eV is not present) and CsPb(Br/I):Cd 20 mol% are shown in Figure 3.7. The remaining absorbance profiles are presented in Annex C.

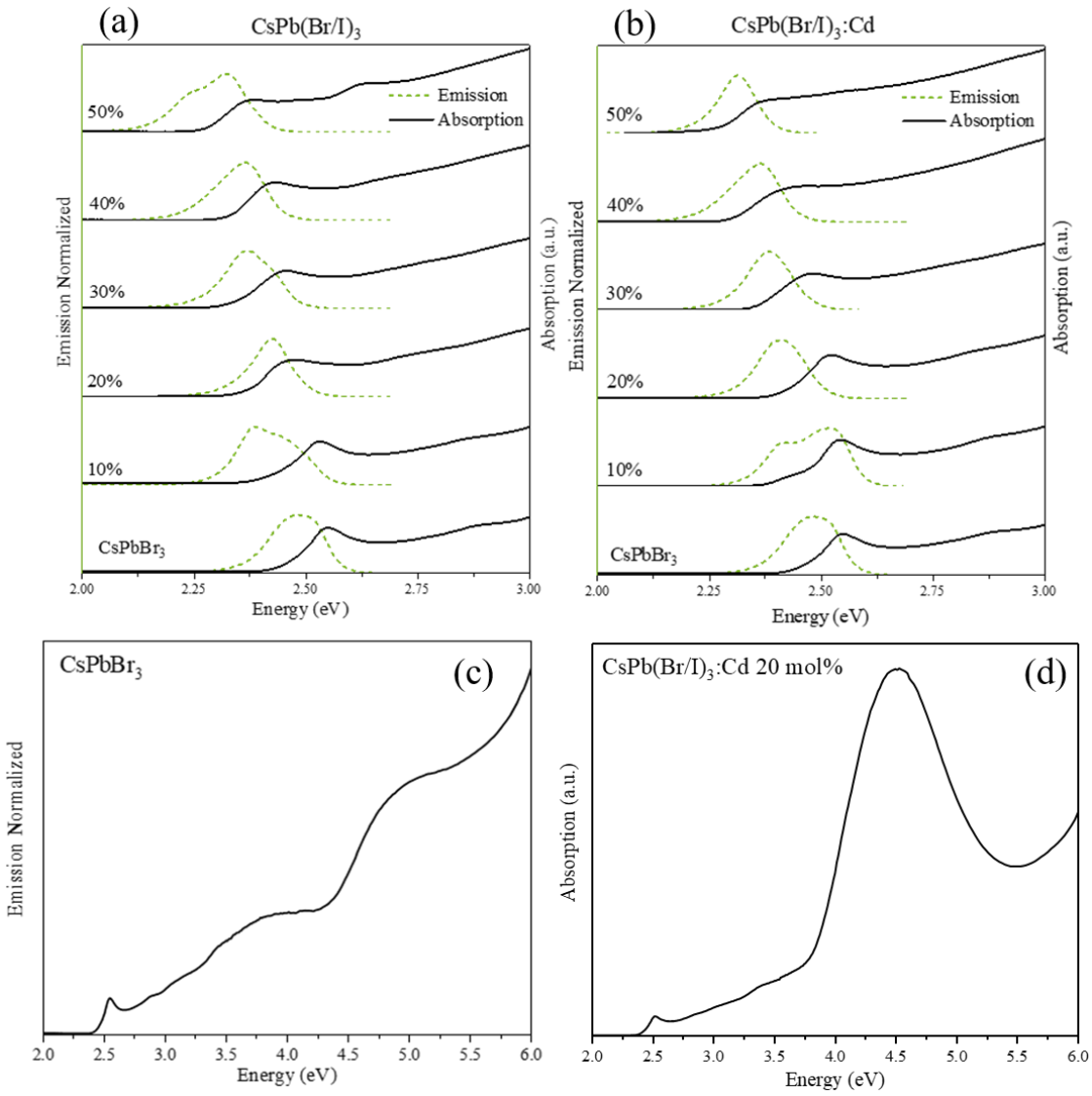

Figure 3.7 Absorption and emission (λ_{exc} = 450 nm) profiles; (a) normalized photoluminescence emission spectrum for $CsPb(Br/I)_3$ with a Br/I ratio of 10, 20, 30, 40 and 50 mol%; (b) normalized photoluminescence emission spectrum for $CsPb(Br/I)_3$:Cd with 10, 20, 30, 40 and 50 mol% of CdI_2; (c) absorbance spectrum for $CsPbBr_3$ sample; (d) absorbance spectrum for $CsPb(Br/I)_3$:Cd 20 mol% sample. The latter shows the absorbance band in the 4 to 5 eV region (250-300 nm).

Table 3.4 Summary table with the obtained emission peaks, FWHM, bandgap and PLQYs of the diluted samples.

Samples	Emission peak (eV)	FWHM (eV)	Bandgap (eV)	PLQY (%)
$CsPbBr_3$	2.48	0.140	2.49	56
$CsPb(Br/I)_3$:Cd 10 mol%	2.52	0.218	2.48	43
$CsPb(Br/I)_3$ 10 mol%	2.38	0.164	2.46	12
$CsPb(Br/I)_3$:Cd 20 mol%	2.41	0.124	2.45	18
$CsPb(Br/I)_3$ 20 mol%	2.42	0.099	2.39	25
$CsPb(Br/I)_3$:Cd 30 mol%	2.39	0.117	2.38	13
$CsPb(Br/I)_3$ 30 mol%	2.37	0.134	2.36	15
$CsPb(Br/I)_3$:Cd 40 mol%	2.35	0.113	2.32	22
$CsPb(Br/I)_3$ 40 mol%	2.36	0.129	2.35	13
$CsPb(Br/I)_3$:Cd 50 mol%	2.32	0.111	2.32	39
$CsPb(Br/I)_3$ 50 mol%	2.32	0.163	2.29	7

As previously mentioned, the bandgaps were calculated according to the Tauc relation. As the mol percentage of both CdI_2 and PbI_2, increases, the bandgap decreases. This is expected due to the presence of iodide in the samples – induces a red-shift of the optical properties. The calculated PLQYs are considerably low when compared with the one obtained for $CsPbBr_3$ (which is already lower than the ones reported in literature) – which might be related with a slight degradation of the samples (that were two weeks old by the time of measurement). It is important to remember that the synthetized QDs underwent no purification procedure or surface coating treatment, having been only centrifuged and redispersed in hexane prior to their storage. Further purification and washing steps should lead to improved stability. The sample containing 50 mol% of CdI_2 is the most recent of the set and shows a significantly higher PLQY than most of the remaining doped samples. Only the $CsPb(Br/I)_3$:Cd 10 mol% has a higher PLQY, which is thought to be related with a significant population of $CsPbBr_3$ emitting at 2.52 eV.

As previously mentioned, it is thought that the presence of Cd^{2+} confers some stability to the IPQDs. To better understand this, two samples, $CsPbBr_3$ and $CsPb(Br/I)_3$:Cd 50 mol%, were synthetized at the exact same time and their absorbance profiles were measured in defined time intervals posterior to their fabrication. These are all shown in Figure 3.8. The obtained absorption profiles show a significant difference between those taken immediately after synthesis (0h) and the measurement taken 24 h after synthesis. In both cases, for 0h, the presence of two absorption bands is visible, for the $CsPbBr_3$ this behavior has been previously seen and was thought to be related with the formation of nanoplates. The second peak at around 2.80 eV completely disappears for the $CsPb(Br/I)_3$:Cd 50 mol% (after 48 h there is still a small – barely visible – indication of a second peak) and the obtained profile is very close to the one expected for IPQDs nanocubes. A week after syntheses, one can still see the semblance of a second peak in the $CsPbBr_3$ sample. After this time, the Cd-containing sample showed no observable precipitation, while the blank $CsPbBr_3$ did (Figure 3.8 (c) and (d)). This leads to the belief that, in fact, the presence of Cd^{2+} can contribute to the stability of the IPQDs.

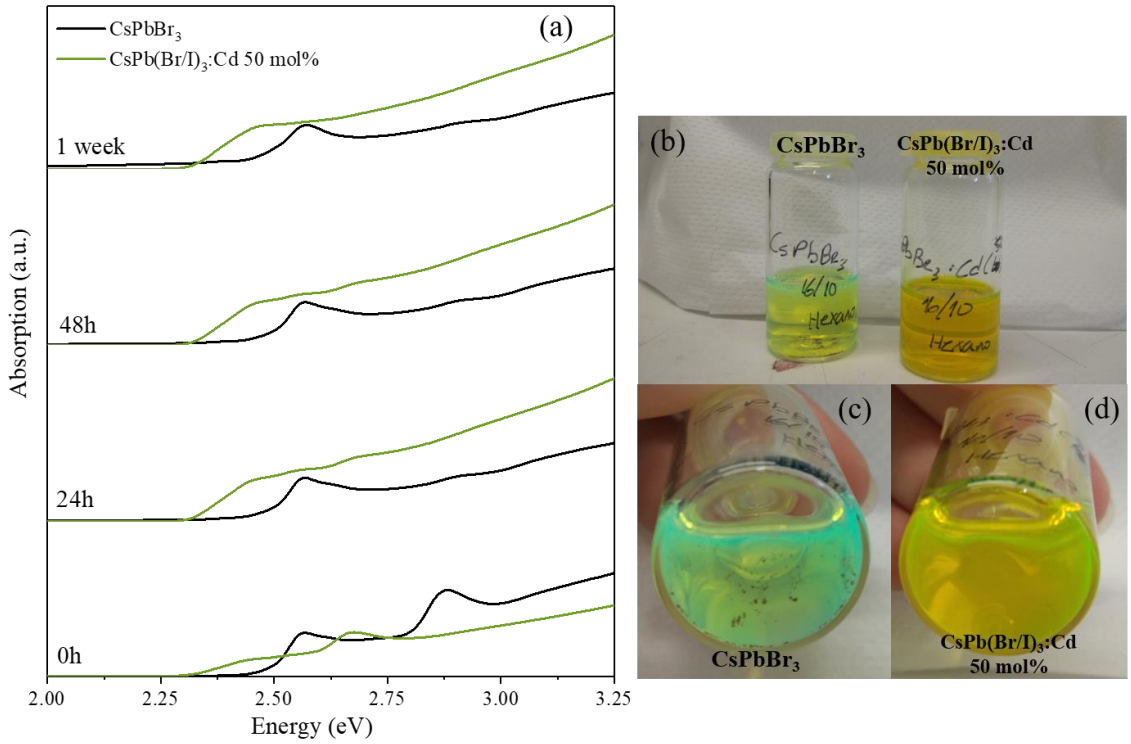

Figure 3.8 Optical properties. (a) Absorption profile for the $CsPbBr_3$ and $CsPb(Br/I)_3$:Cd 50 mol% from as synthetized (0h) to a week old; (b) both samples under ambient light; (c) $CsPbBr_3$ one week old under ambient light – precipitation and degradation signs; (d) $CsPb(Br/I)_3$ one week old under ambient light.

To determine the real quantity of Cd^{2+} in the samples, inductively coupled plasma atomic emission spectroscopy (ICP-AES) was performed (for CsPb(Br/I):Cd 10 and 30 mol%) and the obtained results are presented in Table 3.5.

Table 3.5 Comparison of nominal Cd^{2+} doping content and actual Cd^{2+} doping content determined by ICP-AES.

Samples	Nominal Cd^{2+} (mol%)	Actual Cd^{2+} (mol%)	Reference
$CsPb(Br/I)_3$:Cd	10	0.26	This work
$CsPb(Br/I)_3$:Cd	30	2.47	This work
$CsPbBr_3$:Cd	40	0.8	[35]

It is observable that in literature 2% of the inserted amount is introduced in the perovskite structure (post-synthesis cation exchange doping method) [35], in the case employed in this work, for CsPb(Br/I):Cd 10 mol% sample 2.6% of the nominal amount is present in the final compound and, for $CsPb(Br/I)_3$:Cd 30 mol% sample 8.23% is included in the perovskite structure. The method here reported appears to be more effective in incorporating the metal into the final product when compared with post-synthesis cation exchange method shown in literature. It is important to notice that in literature, reports of doping in IPQDs are accomplished with the use of $CdBr_2$, and the presence of iodide might also contribute to the performance of this method.

3.3.2. Cd-doping in iodide-based samples: optical properties

To better understand the influence of Cd^{2+} in the optical properties of the IPQDs the synthesis of $CsPbI_3$ was performed. The bandgaps were calculated following the Tauc relation and, alongside the emission peaks, FWHM and PLQYs, are presented in Table 3.6. The obtained absorption and emission profiles are shown in Figure 3.9

Once again, in terms of emission peaks and bandgap the change, even though present, is not very pronounced. Nevertheless, it is observable that the emission profile is cleaner and has a more defined peak (smaller FWHM) for the samples with Cd^{2+}. The PLQYs of the $CsPbI_3$ sample go in accordance with literature (around 58 %) [39]. For the $CsPbI_2$:Cd 50 mol% the PLQY is lower than the one obtained for the $CsPbI_3$ but still significantly high (45 %).

Table 3.6 Summary table with acquired emission peaks, FWHM, bandgaps and PLQYs for both iodide-based samples.

Sample	Emission peak (eV)	FWHM (eV)	Bandgap (eV)	PLQY (%)
$CsPbI_3$	1.81	0.237	1.79	58
$CsPbI_3$:Cd 50 mol%	1.79	0.089	1.77	45

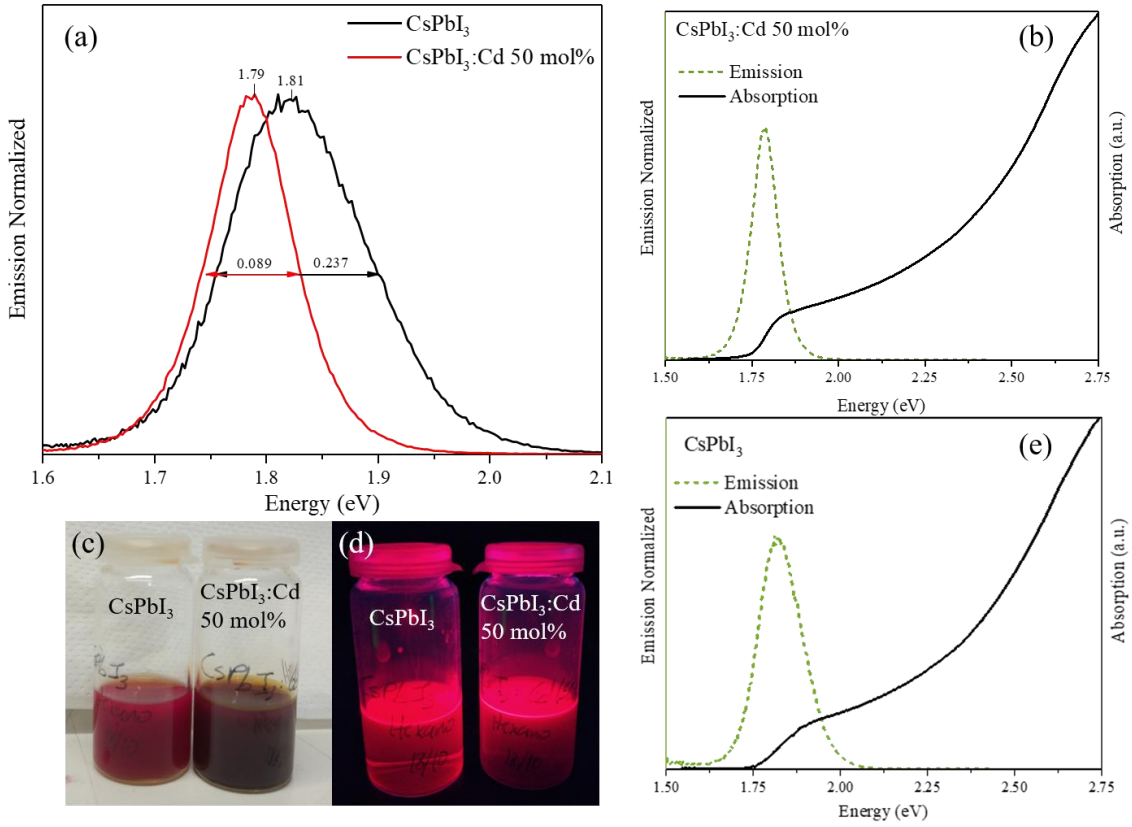

Figure 3.9 Optical properties of iodide-based samples. (a) Photoluminescence emission spectra (λ_{exc} = 500 nm) of $CsPbI_3$ (black line) and $CsPbI_3$:Cd 50 mol% (red line); (b) absorption and emission profile for $CsPbI_3$ sample; (c) both samples under ambient light; (d) both samples under UV light; (e) absorption and emission profile for $CsPbI_3$:Cd 50 mol%.

3.4. Final thoughts and future perspectives

To fully comprehend the optical properties and possibilities of the nanocrystals reported here it is important to note that further studies and measurements are needed. To determine the actual role of Cd^{2+} in the synthesis, $CsPbBr_3$ doped with $CdBr_2$ should be produced and studied, thus eliminating the iodide variable in these compounds.

Further characterization should be done by employing other techniques, starting with time-resolved photoluminescence decays, X-ray diffraction (XRD) – particularly important to determine crystal structure of the samples – and transmission electron microscopy (TEM), for all cases in study. The ICP-AES analysis needs to be employed for more doping concentrations, again for both cases.

The synthesis process can also be improved, adding washing steps or even surface coating, to improve long-term stability – storage under controlled atmosphere will also enhance the long-term behavior. In addition, to confirm if the presence of Cd^{2+} is conferring stability to the IPQDs the optical properties (emission and absorption profiles) have to be studied through longer periods (measured in defined intervals of time) while simultaneously performing XDR.

For future applications, especially for LEDs and solar cells, study of thin films of these materials is important and as solution-based materials, deposition can be performed by spin-coating and optical properties may be studied by absorption and photoluminescence spectra.

4. Conclusion

Two synthesis procedures for IPQDs fabrication were tested – SR and HI method. Both allowed the production of bromide-based luminescent nanoparticles with emission profiles that go in accordance with the ones seen in literature for IPQDs – small FWHM and well-defined peaks at around 2.4 eV (510 nm). While both methods resulted in narrow FWHM, the HI synthesis method lead to a better result (25% smaller). The synthesis of iodide-based IPQDs was only successful following the HI technique. It was observable, and is also in accordance with literature, that the bromide-based samples were considerably more stable than the iodide-based ones. Taking this into account the HI method was chosen and employed for the remaining of the work.

Several metals were tested as dopants for the IPQDs (CdI_2, CuBr and $ZnCl_2$). All of the utilized metals resulted in the synthesis of luminescent nanoparticles. The iodide-based samples presented a strong absorption peak at 3.34 eV (for both Cd-doped and non-doped sample), that completely masked the absorbance peak (only visible when zooming in the 1.77 to 2.5 eV range). This observed band is thought to be linked to the Cs_4PbI_6 phase. Nonetheless, a strong red emission is present in the resulting samples, which indicate the presence of $CsPbI_3$ QDs. The $CsPbBr_3$ sample exhibited interesting absorption properties that are consistent with the presence of nanoplates. These are thought to be result of the necessary dilution steps employed to obtain the required optical density for spectroscopic measurements. The synthesis where the doping procedure was employed, especially the ones doped with CuBr and CdI_2 exhibited absorbance profiles close to those expected of IPQD. The standard $CsPbBr_3$ sample presents a bandgap of 2.49 (closer to that of a nanoplate, 2.52 eV, than the one seen for nanocubes, 2.42 eV) and high PLQY (56 %) – the latter is considerably smaller than the values described in literature, that round the 90 %. The Cu- and Cd-doped variants show redshifted optical properties, while the Zn-doped on the other hand, suffered from a blue-shift. The Cd- doped $CsPbBr_3$ were chosen for the remaining of the work.

A comparative study was designed to examine whether the observed optical properties in the Cd-doped samples were due to the metal or the halide (iodide) which accompanies it. The obtained emission peaks were very similar between the samples doped with PbI_2 and CdI_2 indicating that the red-shift observed is most likely due to the presence of I^-. Nevertheless, it is apparent that the samples containing Cd^{2+} present cleaner and more defined emission peaks with smaller FWHM and generally higher PLQYs, taking the 50 mol% case as an example, the sample with Cd incorporated exhibits a PLQY more than 5 times higher than the non-Cd synthesis.

The presence of Cd^{2+} seems to result in improved stability of the obtained IPQDs. When studying the progression of the absorption properties of doped and undoped samples with time, it is apparent that – a week post-synthesis – the Cd-doped samples still presented properties consistent with those expected of IPQDs. Moreover, while in the undoped $CsPbBr_3$ sample precipitation took place, the Cd-doped sample did not. These empirical observations lead to the belief that indeed the Cd^{2+} is playing some role in the stability of the synthetized compounds. The main sign of improved stability is the observable precipitate on the $CsPbBr_3$ that is not visible for the Cd-doped sample.

ICP-AES analyses was performed for $CsPbBr_3$, $CsPb(Br/I)_3$:Cd with 10 mol% and 30 mol% content of CdI_2. It is observable that the nominal amount is significantly higher than the actual amount of Cd^{2+} (mol%) in the samples. For the $CsPb(Br/I)_3$:Cd 10 mol% sample only 0.26 mol% was present in the QDs structure and for the $CsPb(Br/I)_3$:Cd 30 mol% just 2.47 mol% was introduced in the structure.

To better understand the influence of CdI_2 in the optical properties of the IPQDs the synthesis of $CsPbI_3$ and $CsPbI_3$:Cd 50 mol% was performed. Once again, in terms of emission peak and bandgap a significant shift is not observed (non-doped emission peak and bandgap were 1.81 eV and 1.79 eV, respectively, and for the Cd-doped sample were 1.79 eV and 1.77 eV). The most observable change is in the FWHM, which is much smaller in the 50 mol% Cd-doped case – 0.089 versus 0.237 eV. The PLQY of non-doped and doped samples were 58 % and 45 %, correspondingly.

Further studies are required to fully understand the real influence of Cd^{2+} in the morphological, optical and stability properties. Nevertheless, the presence of well define emission peaks, as well as absorption profiles close to those expected from typical IPQDs are observed. Stability is one of the main problems in perovskites in general (although the inorganic counterparts are more stable than OIHPs) – the presence of Cd^{2+} in the synthesis seems to confer some stability and improved emission profiles, for both iodide and bromide-based samples.

5. References

[1] T. M. Brenner, D. A. Egger, L. Kronik, G. Hodes, and D. Cahen, "Hybrid organic—inorganic perovskites: low-cost semiconductors with intriguing charge-transport properties," *Nat. Rev. Mater.*, p. 16011, 2016.

[2] J. Song, J. Li, X. Li, L. Xu, Y. Dong, and H. Zeng, "Quantum Dot Light-Emitting Diodes Based on Inorganic Perovskite Cesium Lead Halides (CsPbX3)," *Adv. Mater.*, vol. 27, no. 44, pp. 7162–7167, 2015.

[3] Q. Chen *et al.* , "Under the spotlight: The organic-inorganic hybrid halide perovskite for optoelectronic applications," *Nano Today*, vol. 10, no. 3, pp. 355–396, 2015.

[4] K. Hong, Q. Van Le, S. Y. Kim, and H. W. Jang, "Low-dimensional halide perovskites: Review and issues," *J. Mater. Chem. C*, vol. 6, no. 9, pp. 2189–2209, 2018.

[5] Akihiro Kojima, K. Teshima, Y. Shirai, and T. Miyasaka, "Organometal Halide Perovskites as Visible- Light Sensitizers for Photovoltaic Cells," *J. Am. Chem. Soc.*, vol. 131, pp. 6050–6051, 2009.

[6] N. Wang, W. Liu, and Q. Zhang, "Perovskite-Based Nanocrystals: Synthesis and Applications beyond Solar Cells," *Small Methods*, vol. 2, no. 6, p. 1700380, 2018.

[7] L. C. Schmidt *et al.* , "Nontemplate Synthesis of $CH_3NH_3PbBr_3$ Perovskite Nanoparticles," *J. Am. Chem. Soc.*, vol. 136, no. 3, pp. 850–853, 2014.

[8] Y. Wang and H. Sun, "All-Inorganic Metal Halide Perovskite Nanostructures: From Photophysics to Light-Emitting Applications," *Small Methods*, vol. 1700252, p. 1700252, 2017.

[9] C. de Weerd, T. Gregorkiewicz, and L. Gomez, "All-Inorganic Perovskite Nanocrystals: Microscopy Insights in Structure and Optical Properties," *Adv. Opt. Mater.*, vol. 1800289, p. 1800289, 2018.

[10] L. Protesescu *et al.* , "Nanocrystals of Cesium Lead Halide Perovskites (CsPbX3, X = Cl, Br, and I): Novel Optoelectronic Materials Showing Bright Emission with Wide Color Gamut," *Nano Lett.*, vol. 15, no. 6, pp. 3692–3696, 2015.

[11] J. Zhang *et al.* , "Low-Dimensional Halide Perovskites and Their Advanced Optoelectronic Applications," *Nano-Micro Lett.*, vol. 9, no. 3, pp. 1–26, 2017.

[12] S. Adjokatse, H. H. Fang, and M. A. Loi, "Broadly tunable metal halide perovskites for solid-state light-emission applications," *Mater. Today*, vol. 20, no. 8, pp. 413–424, 2017.

[13] J. J. Choi and S. J. L. Billinge, "Perovskites at the nanoscale: From fundamentals to applications," *Nanoscale*, vol. 8, no. 12, pp. 6206–6208, 2016.

[14] M. A. Green, A. Ho-Baillie, and H. J. Snaith, "The emergence of perovskite solar cells" *Nat. Photonics*, vol. 8, no. 7, pp. 506–514, 2014.

[15] X. He, Y. Qiu, and S. Yang, "Fully-Inorganic Trihalide Perovskite Nanocrystals : A New Research Frontier of Optoelectronic Materials," *Advanced Materials*, vol. 1700775, pp. 1–27, 2017.

[16] Q. A. Akkerman, G. Rainò, M. V. Kovalenko, and L. Manna, "Genesis, challenges and opportunities for colloidal lead halide perovskite nanocrystals," *Nat. Mater.*, vol. 17, no. 5, pp. 394–405, 2018.

[17] D. Weber, "$CH_3NH_3PbX_3$, ein Pb(II)-System mit kubischer Perowskitstruktur," vol. 1445, no. August 1978, pp. 1443–1445, 2015.

[18] P. Fu *et al.* , "Perovskite nanocrystals: synthesis, properties and applications," *Sci. Bull.*, vol. 62, no. 5, pp. 369–380, 2017.

[19] B. Luo, B. Naghadeh, and J. Z. Zhang, "Lead Halide Perovskite Nanocrystals: Stability , Surface Passivation , and Structural Control," *Chem. Nano. Mat.*, vol. 95064, pp. 456–465, 2017.

[20] S. González, C. Julia, and P. Prieto, "Colloidal photoemissive nanoparticles," *ChemTexts*, vol 4, pp. 8, 2018.

[21] Y. Iso and T. Isobe, "Review — Synthesis , Luminescent Properties, and Stabilities of Cesium Lead Halide Perovskite Nanocrystals," *ECS Jornal of Solid State Science and Technologie*, vol. 7, no. 1, pp. 3040–3045, 2018.

[22] M. V Kovalenko, L. Protesescu, and M. I. Bodnarchuk, "Properties and potential optoelectronic applications of lead halide perovskite nanocrystals," *Science mag., vol.* 750, no. November, pp. 745–750, 2017.

[23] M. A. Reed, R. J. Aggarwal, R. J. Matyi, T. M. Moore, and A. E. Wetsel, "Observations of Discrete Electronic States in a Zero-dimensional Semiconductor Nanostructure," *Physical Review*, vol. 60, no. 6, 1988.

[24] Y. Zhang, J. Liu, Z. Wang *et al.*, "Synthesis, properties, and optical applications of low-dimensional perovskites" *Chem. Commun.*, vol. 52, pp. 13637–13655, 2016.

[25] A. P. Alivisatos, N. Series, and N. Feb, "Semiconductor Clusters , Nanocrystals , and Quantum Dots," vol. 271, no. 5251, pp. 933–937, 2007.

[26] H. H. Ma, M. Imran, Z. Dang, and Z. Hu, "Growth of Metal Halide Perovskite , from Nanocrystal to Micron-Scale Crystal : A Review," *Crystals*, pp. 1–25, 2018.

[27] C. B. Murray, D. J. Norris, and M. G. Bawendi, "Synthesis and Characterization of Nearly Monodisperse CdE (E = S, Se, Te) Semiconductor Nanocrystallites," *J. Am. Chem. Soc.*, vol. 115, no. 19, pp. 8706–8715, 1993.

[28] C. De Mello Donegá, P. Liljeroth, and D. Vanmaekelbergh, "Physicochemical evaluation of the hot-injection method, a synthesis route for monodisperse nanocrystals," *Small*, vol. 1, no. 12, pp. 1152–1162, 2005.

[29] X. Li *et al.* , "$CsPbX_3$ Quantum Dots for Lighting and Displays: Room temperature Synthesis, Photoluminescence Superiorities, Underlying Origins and White Light-Emitting Diodes," *Adv. Funct. Mater.*, vol. 26, no. 15, pp. 2435–2445, 2016.

[30] P. Fu *et al.* , "Perovskite nanocrystals: synthesis, properties and applications," *Sci. Bull.*, vol. 62, no. 5, pp. 369–380, 2017.

[31] T. C. Jellicoe *et al.* , "Synthesis and Optical Properties of Lead-Free Cesium Tin Halide Perovskite Nanocrystals," *J. Am. Chem. Soc.*, vol. 138, no. 9, pp. 2941–2944, 2016.

[32] N. K. Noel *et al.* , "Lead-free organic–inorganic tin halide perovskites for photovoltaic applications," *Energy Environ. Sci.*, vol. 7, no. 9, pp. 3061–3068, 2014.

[33] W. Liu *et al.* , "Mn^{2+} - Doped Lead Halide Perovskite Nanocrystals with Dual-Color Emission Controlled by Halide Content," *J. Am. Chem. Soc.*, vol. 138, no. 45, pp. 14954–14961, 2016.

[34] W. Van Der Stam *et al.* , "Highly Emissive Divalent-Ion-Doped Colloidal $CsPb_{1-x}M_xBr_3$ Perovskite Nanocrystals through Cation Exchange," *J. Am. Chem. Soc.*, 2017.

[35] S. Zou *et al.* , "Stabilizing Cesium Lead Halide Perovskite Lattice through Mn(II) Substitution for Air-Stable Light-Emitting Diodes," *J. Am. Chem. Soc.*, vol. 139, no. 33, pp. 11443–11450, 2017.

[36] F. Zhang *et al.* , "Brightly luminescent and color-tunable colloidal $CH_3NH_3PbX_3$ (X = Br, I, Cl) quantum dots: Potential alternatives for display technology," *ACS Nano*, vol. 9, no. 4, pp. 4533–4542, 2015.

[37] C. Lu *et al.* , "Enhanced stabilization of inorganic cesium lead triiodide ($CsPbI_3$) perovskite quantum dots with tri-octylphosphine," *Nano Res.*, vol. 11, no. 2, pp. 762–768, 2018.

[38] Q. A. Akkerman, A. L. Abdelhady, and L. Manna, "Zero-Dimensional Cesium Lead Halides: History, Properties, and Challenges," *J. Phys. Chem. Lett.*, vol. 9, pp. 2326–2337, 2018.

[39] M. Imran *et al.* , "Benzoyl Halides as Alternative Precursors for the Colloidal Synthesis of Lead-Based Halide Perovskite Nanocrystals," *J. Am. Chem. Soc.*, vol. 140, no. 7, pp. 2656–2664, 2018.

[40] F. Palazon *et al.* , "Postsynthesis Transformation of Insulating Cs_4PbBr_6 Nanocrystals into Bright Perovskite $CsPbBr_3$ through Physical and Chemical Extraction of CsBr," *ACS Energy Lett.*, vol. 2, no. 10, pp. 2445–2448, 2017.

[41] Y. Bekenstein, B. A. Koscher, S. W. Eaton, P. Yang, and A. P. Alivisatos, "Highly Luminescent Colloidal Nanoplates of Perovskite Cesium Lead Halide and Their Oriented Assemblies," *J. Am.*

Chem. Soc., vol. 137, no. 51, pp. 16008–16011, 2015.

[42] Y. Tong *et al.* , "Dilution-Induced Formation of Hybrid Perovskite Nanoplatelets," *ACS Nano*, vol. 10, no. 12, pp. 10936–10944, 2016.

[43] J. H. Cha *et al.* , "Photoresponse of $CsPbBr_3$ and Cs_4PbBr_6 Perovskite Single Crystals," *J. Phys. Chem. Lett.*, vol. 8, no. 3, pp. 565–570, 2017.

[44] A. Kirakosyan, S. Yun, S. G. Yoon, and J. Choi, "Surface engineering for improved stability of $CH_3NH_3PbBr_3$ perovskite nanocrystals," *Nanoscale*, vol. 10, no. 4, pp. 1885–1891, 2018.

6. Annex A – ICP-AES

The metal content was determined by ICP-AES. The analysis was carried out on a Horiba Jobin Yvon ULTIMA sequential ICP, using the Horiba Jobin Yvon ICP Analyst 5.4 software.

The chosen wavelengths were:

Table 6.1 Measurements wavelengths

Element	Wavelength (nm)
Cd	226.502
Pb	220.353

Instrument configuration and general experimental conditions are summarized in. For each sample three determinations were performed, and the average results were reported.

Table 6.2 Analytical ICP-AES conditions

Instrument	ICP Ultima
RF generator power	1.05 kw
RF frequency	40.68 MHz
Plasma gas flowrate	12 L/min
Carrier gas flowrate	1.0 L/min
Sample introduction	Miramist nebulizer
Misting chamber	Cyclonic glass chamber
Observation method	Radial
Injector tube diameter	3 mm

7. Annex B – Tauc Plot

Here are presented the Tauc Plots for all samples and the respective bandgap. The value of n was set to 1/2 – value for direct and allowed transitions – for all samples.

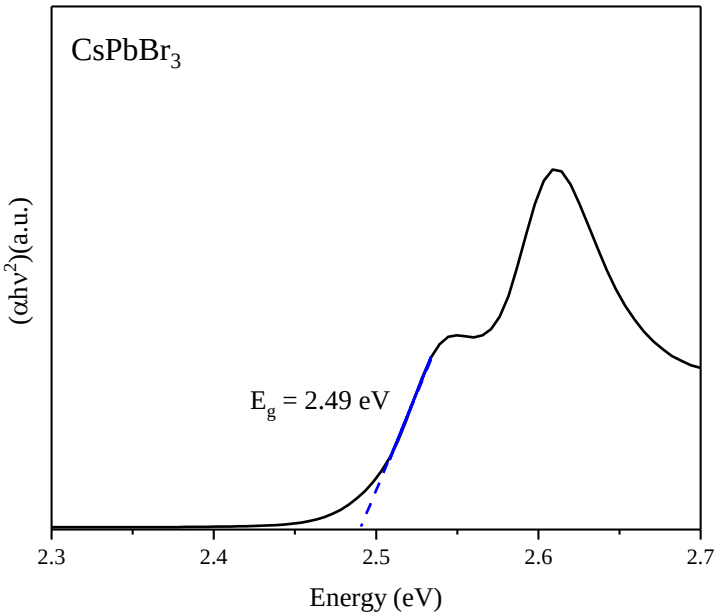

Figure 7.1 Tauc plot for the $CsPbBr_3$ that presented the absorption profile found in nanoplates – thought to be related with dilution

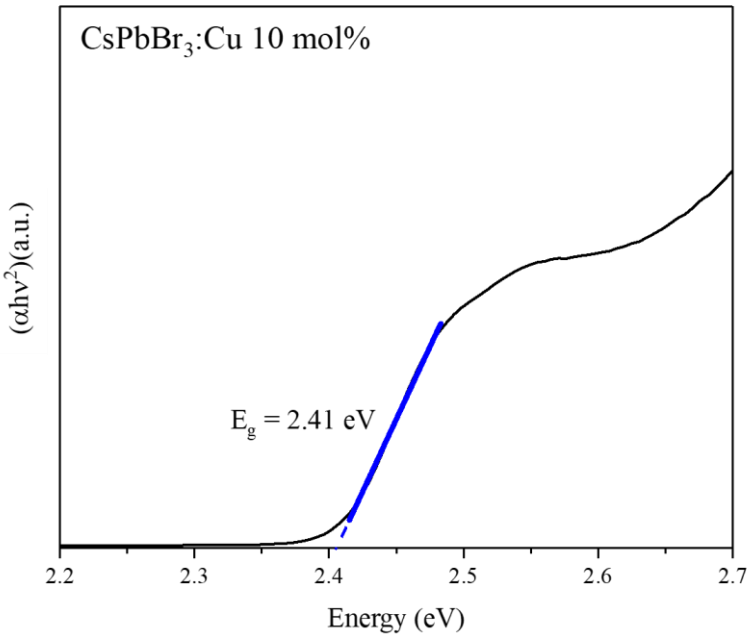

Figure 7.2 Tauc plot for $CsPbBr_3$:Cu 10 mol% sample.

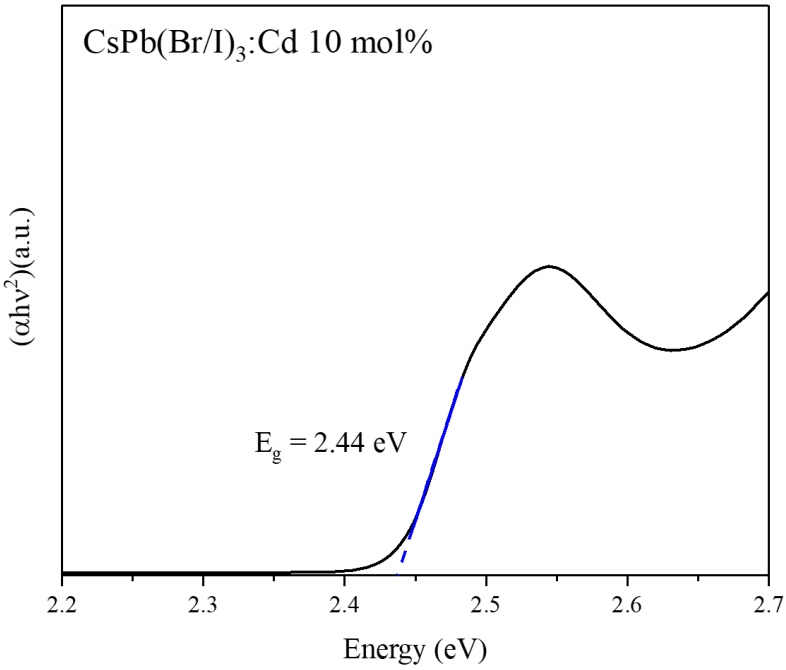

Figure 7.3 Tauc plot for the CsPb(Br/I)$_3$:Cd 10 mol% sample.

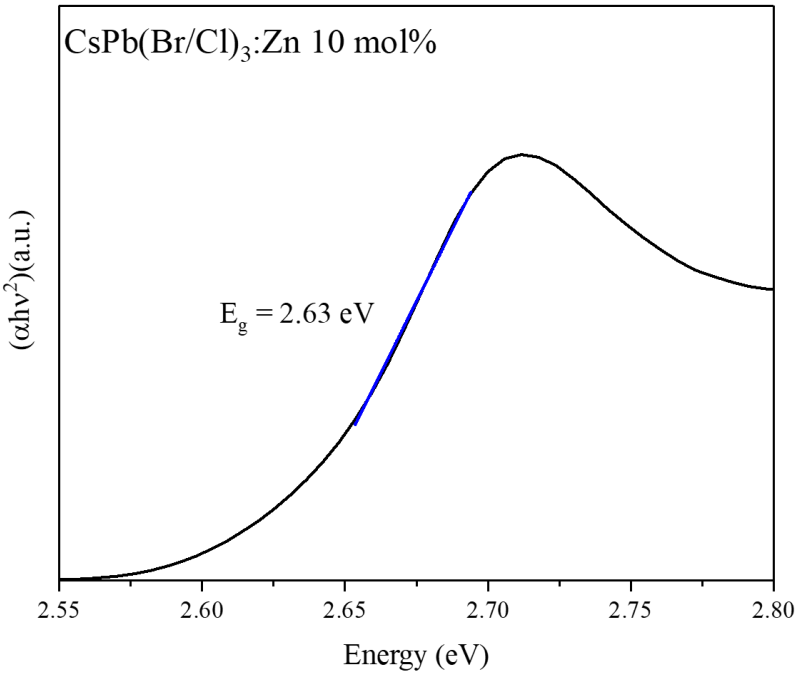

Figure 7.4 Tauc plot for the CsPb(Br/Cl)$_3$:Zn 10 mol% sample.

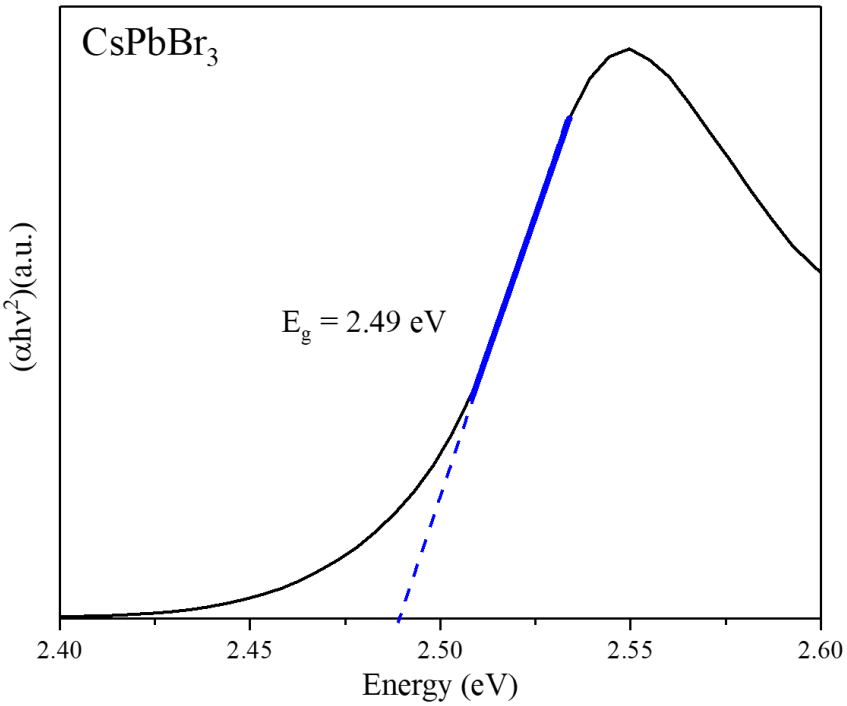

Figure 7.5 Tauc plot for the $CsPbBr_3$ sample – the profile is similar to the one seen in nanocubes.

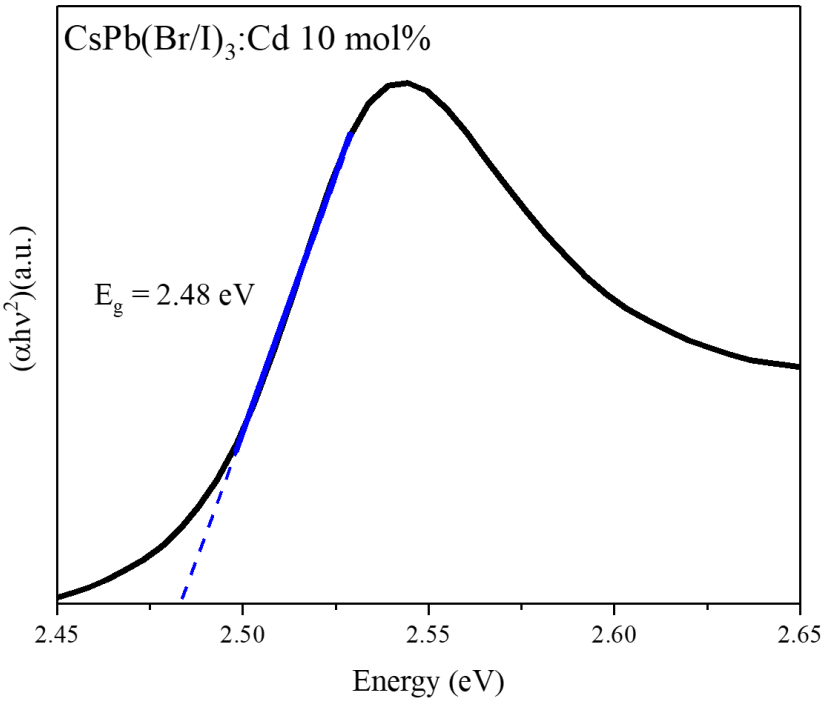

Figure 7.6 Tauc plot for the $CsPb(Br/I)_3$:Cd 10 mol% sample.

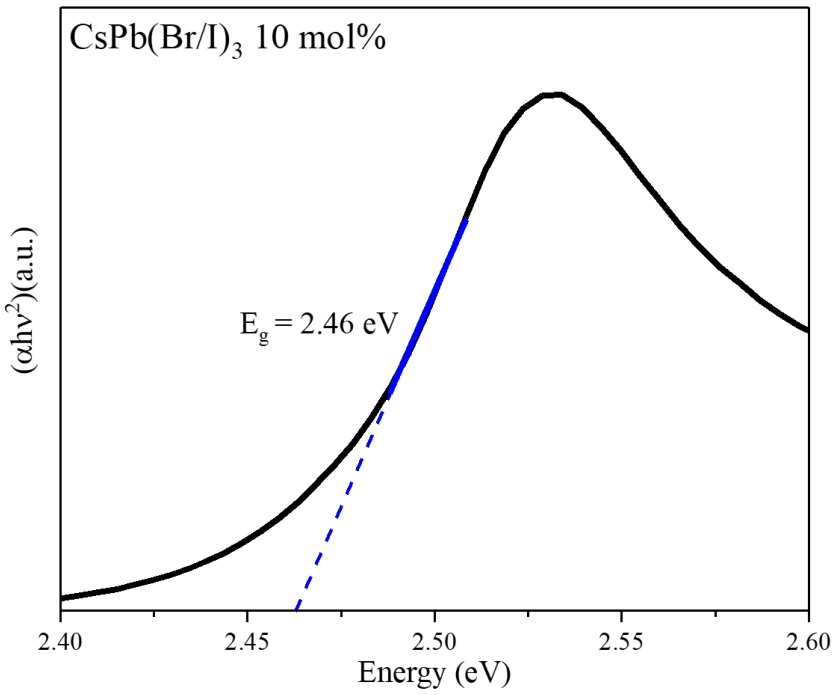

Figure 7.7 Tauc plot for the CsPb(Br/I)$_3$ 10 mol% sample.

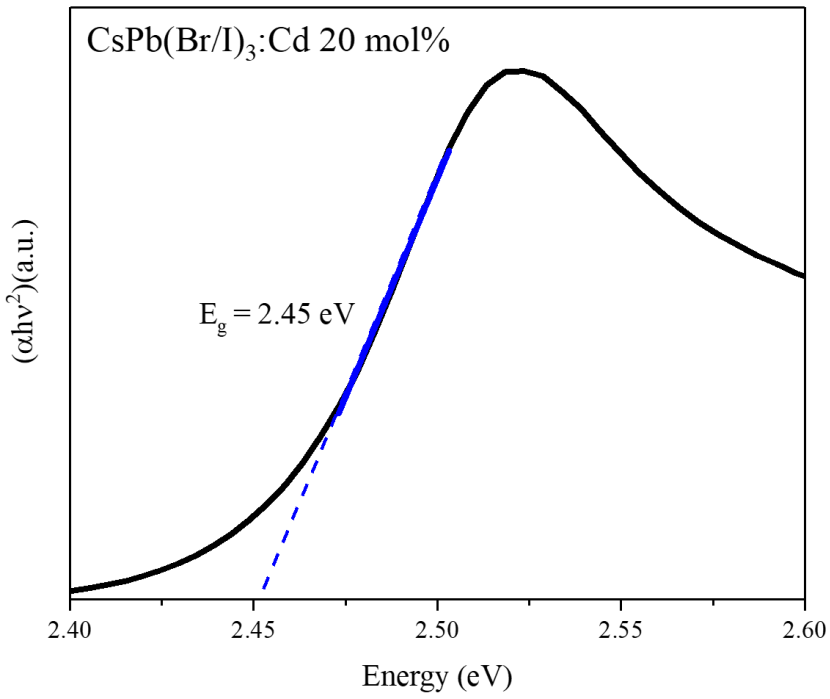

Figure 7.8 Tauc plot for the CsPb(Br/I)$_3$:Cd 20 mol% sample.

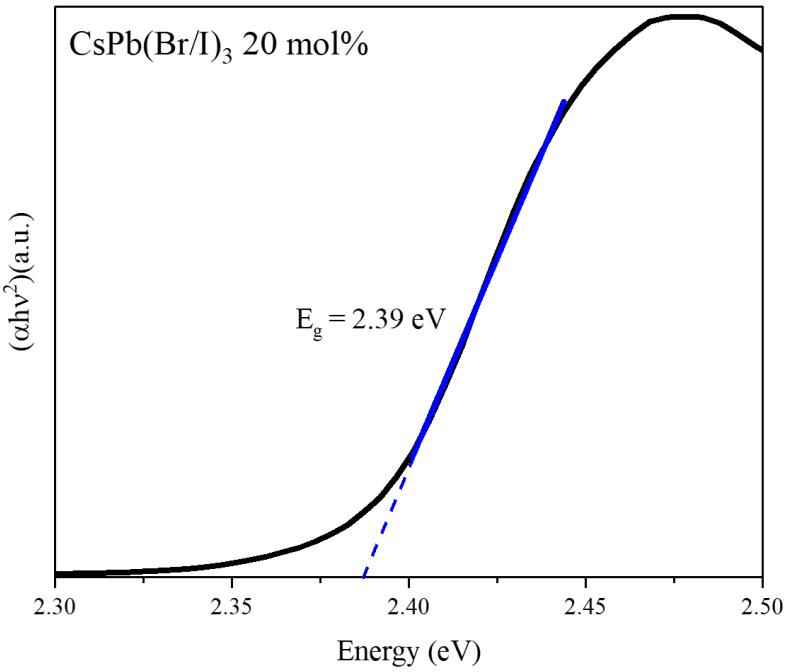

Figure 7.9 Tauc plot for the CsPb(Br/I)$_3$ 20 mol% sample.

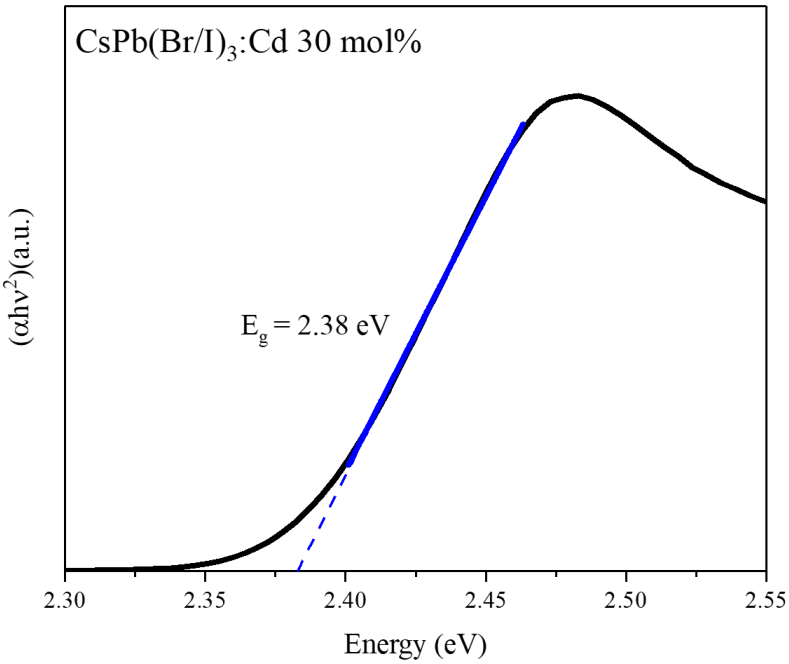

Figure 7.10 Tauc plot for the CsPb(Br/I)$_3$:Cd 30 mol% sample.

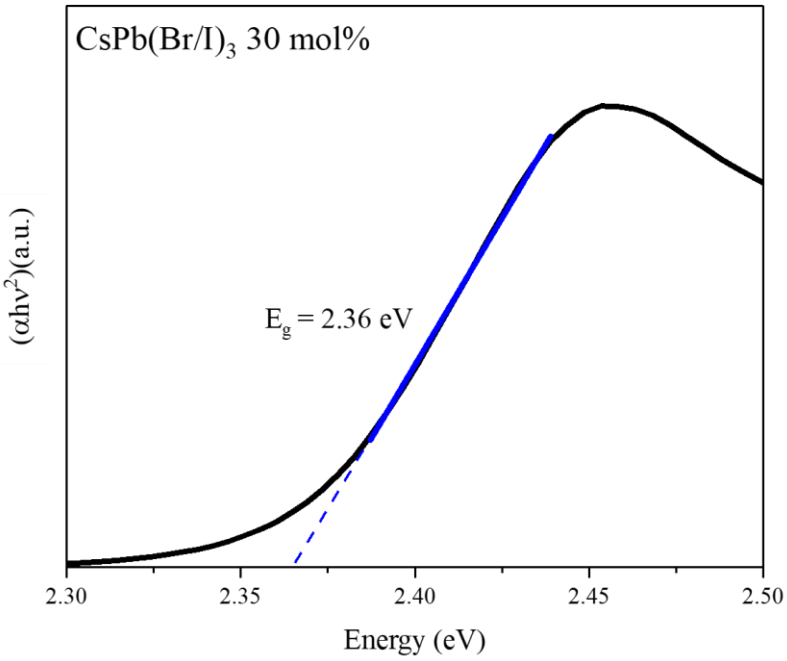

Figure 7.11 Tauc plot for the CsPb(Br/I)$_3$ 30 mol% sample.

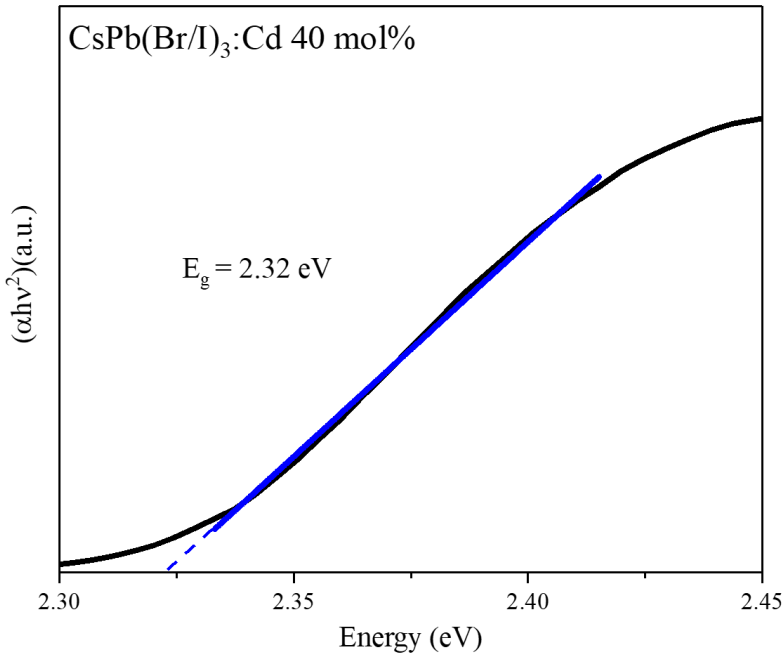

Figure 7.12 Tauc plot for the CsPb(Br/I)$_3$:Cd 40 mol% sample.

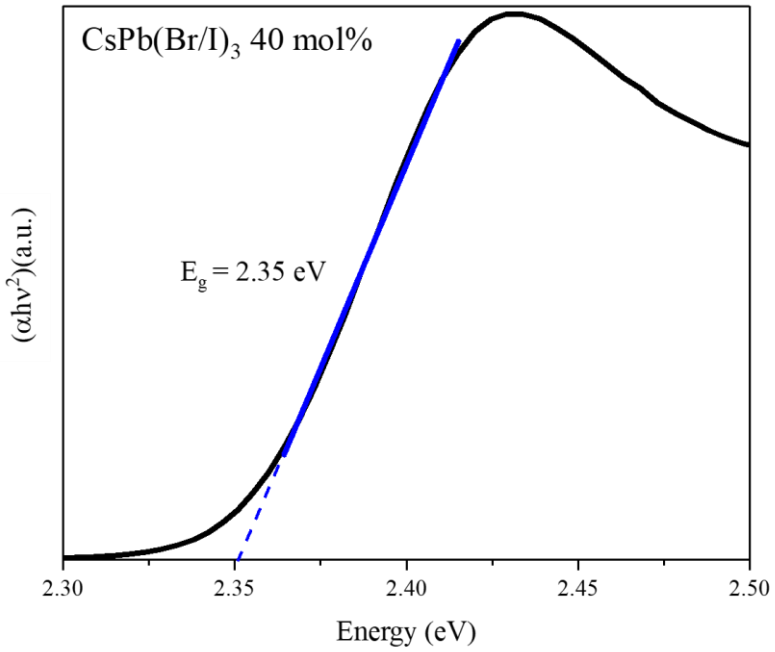

Figure 7.13 Tauc plot for the CsPb(Br/I)$_3$ 40 mol% sample.

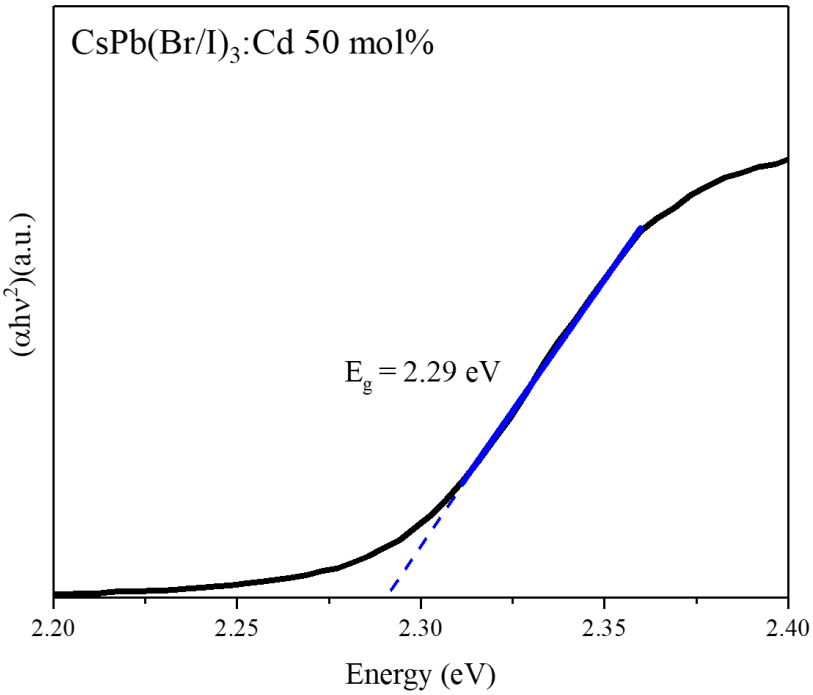

Figure 7.14 Tauc plot for the CsPb(Br/I)$_3$:Cd 50 mol% sample.

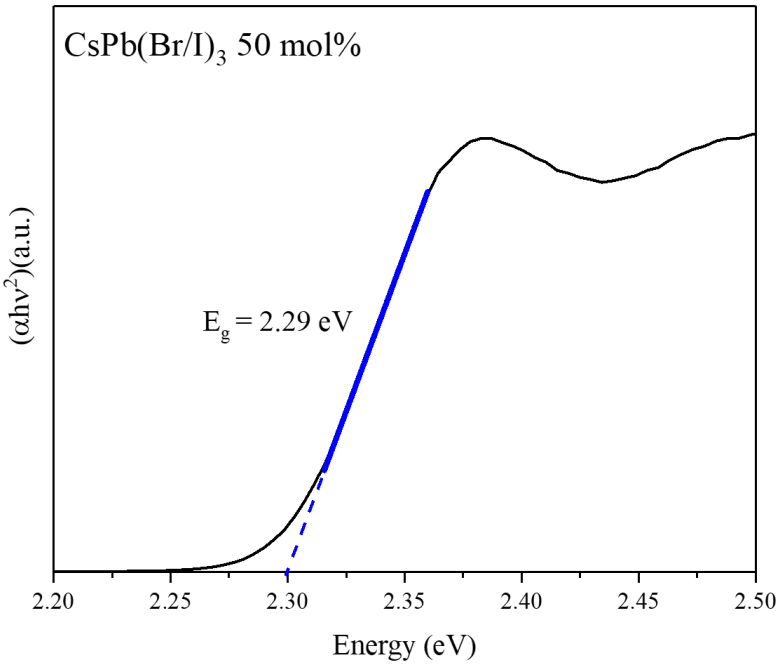

Figure 7.15 Tauc plot for the $CsPb(Br/I)_3$ 50 mol% sample.

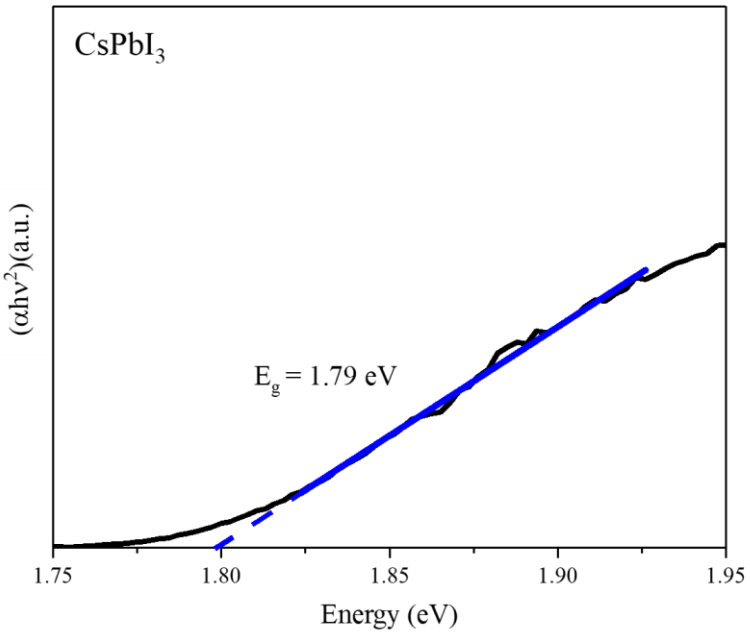

Figure 7.16 Tauc plot for the $CsPbI_3$ sample.

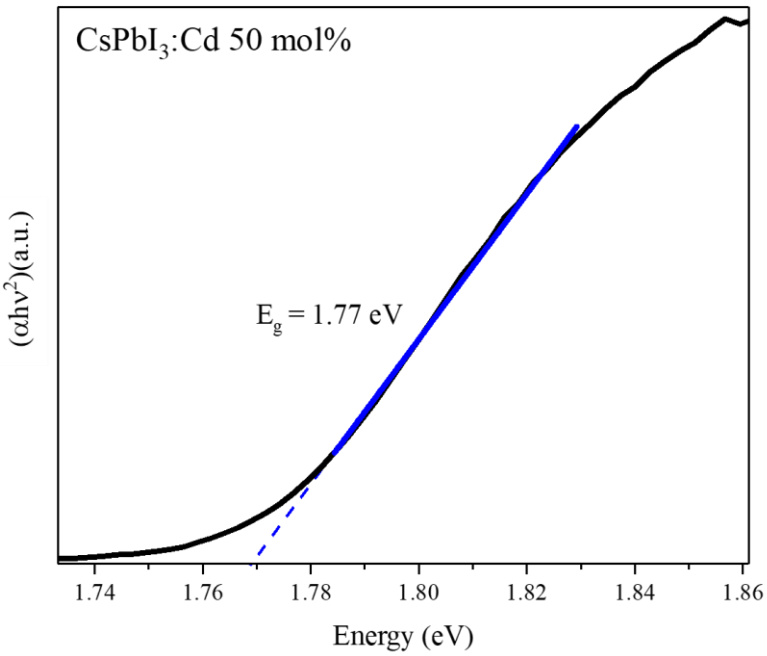

Figure 7.17 Tauc plot for the $CsPbI_3$:Cd 50 mol% sample.

8. Annex C – Absorption Profile

Here the absorption profiles of the Cd-doped and non-doped samples are presented, being visible the presence of the band though to be related with Cs_4PbBr_6 (for bromide-based samples) and Cs_4PbI_6 (for the iodide-based samples).

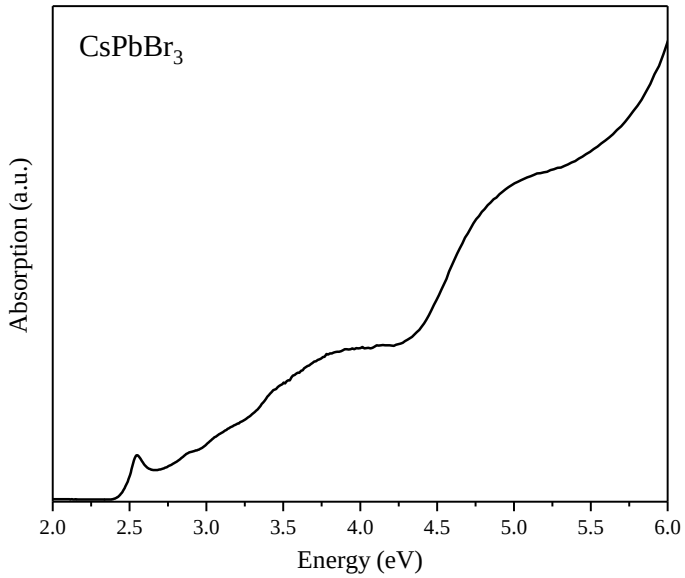

Figure 8.1Absorption profile for the $CsPbBr_3$ sample.

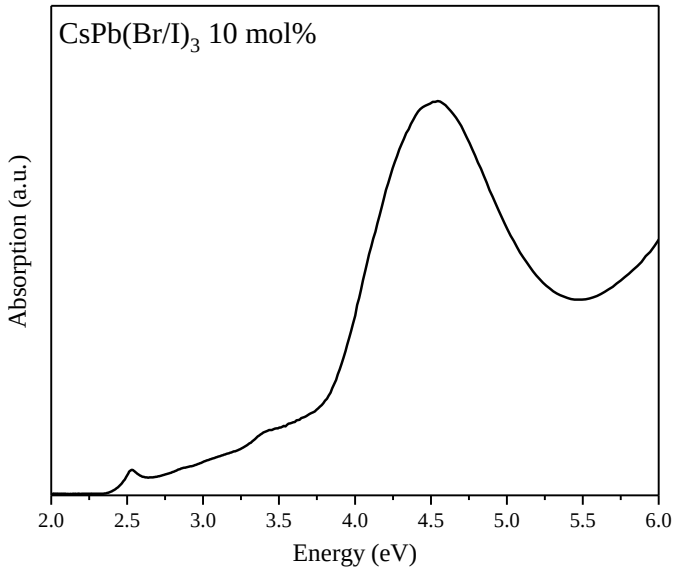

Figure 8.2 Absorption profile for the $CsPb(Br/I)_3$ 10 mol % sample.

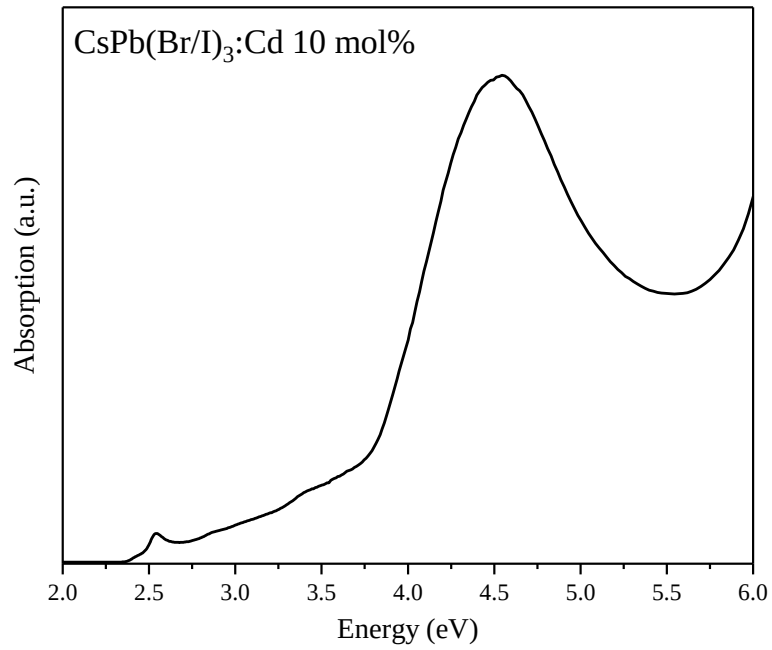

Figure 8.3 Absorption profile for the CsPb(Br/I)3:Cd 10 mol % sample.

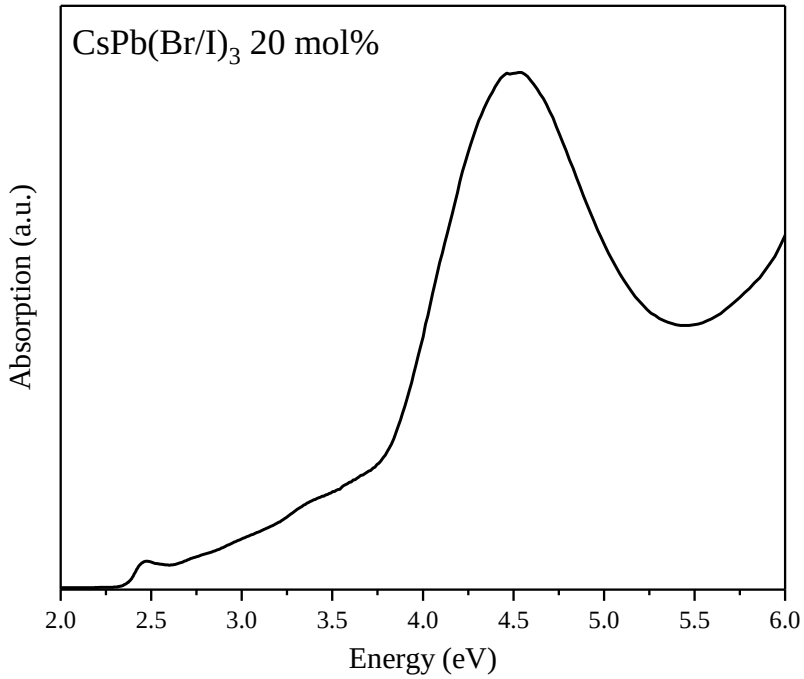

Figure 8.4 Absorption profile for the CsPb(Br/I)3 20 mol % sample.

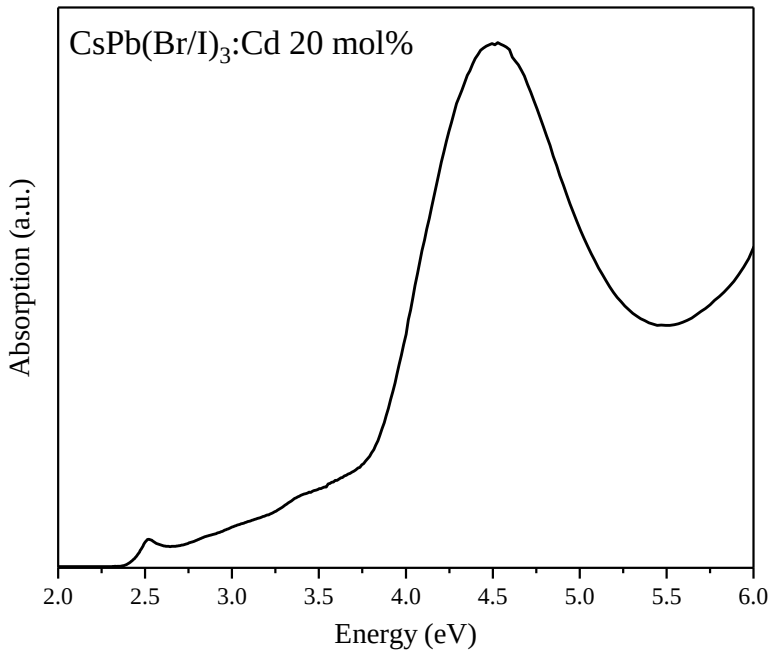

Figure 8.5 Absorption profile for the $CsPb(Br/I)_3$Cd 20 mol % sample.

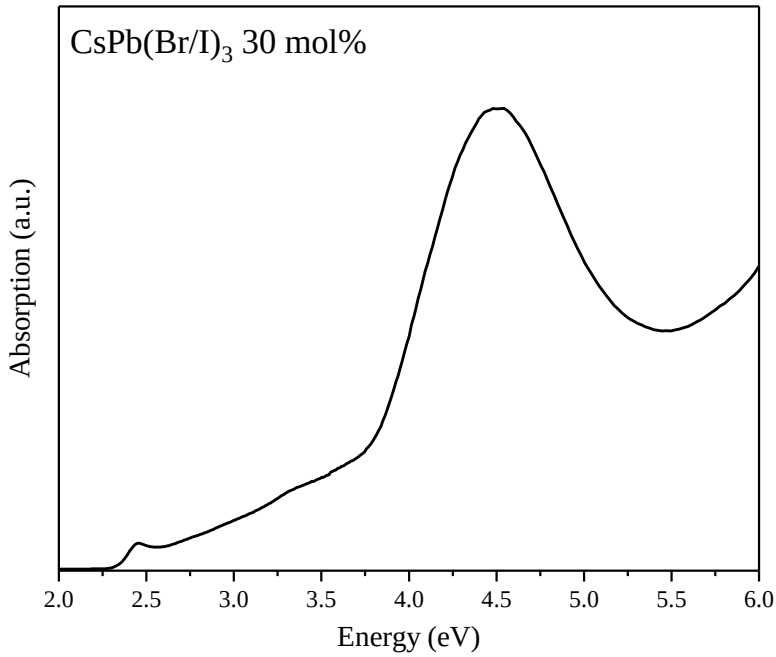

Figure 8.6 Absorption profile for the $CsPb(Br/I)_3$ 30 mol % sample.

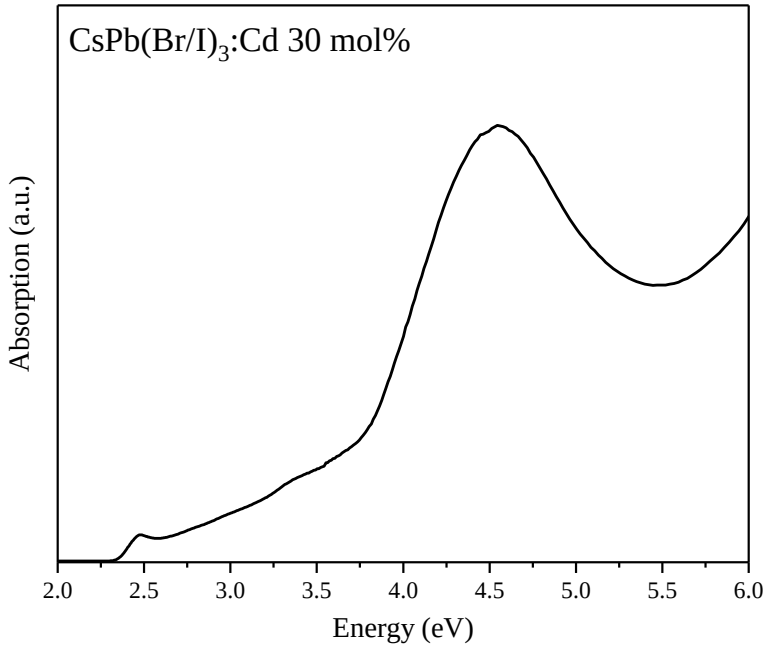

Figure 8.7 Absorption profile for the $CsPb(Br/I)_3$:Cd 30 mol % sample.

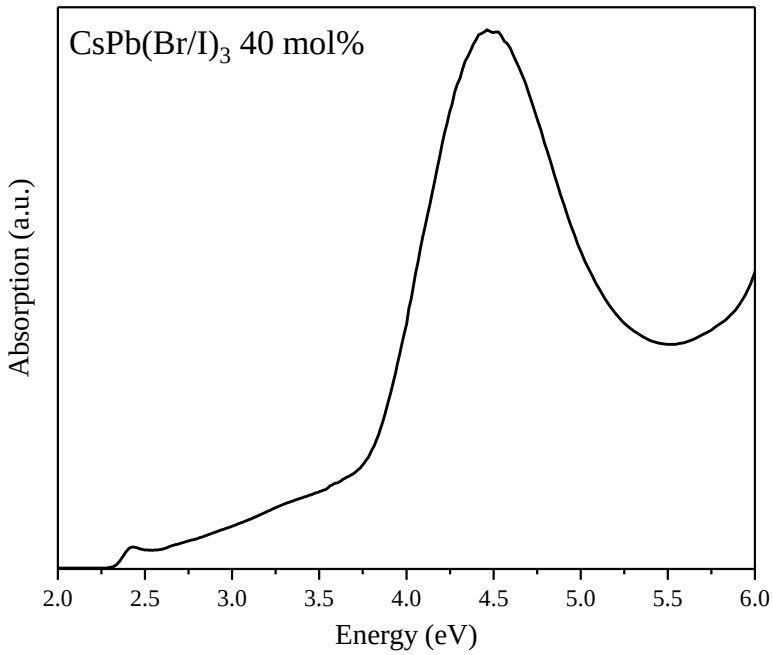

Figure 8.8 Absorption profile for the $CsPb(Br/I)_3$ 40 mol % sample.

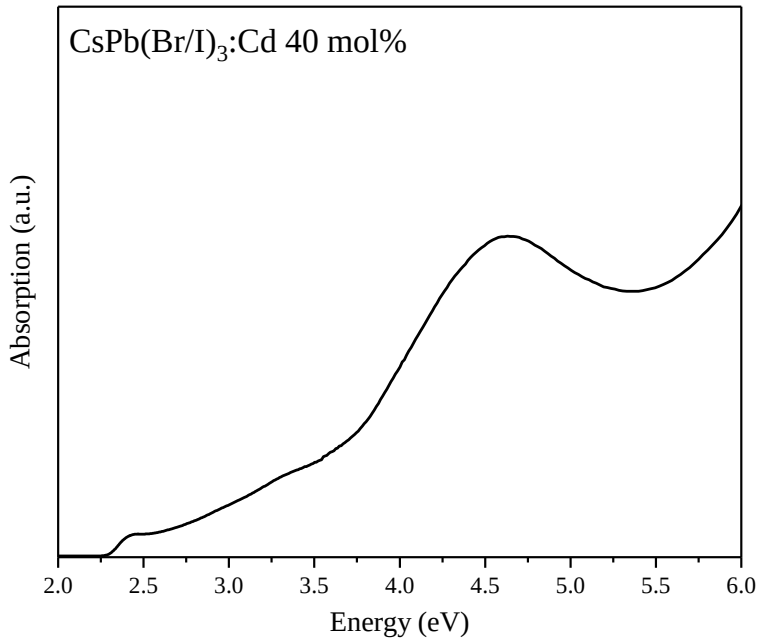

Figure 8.9 Absorption profile for the CsPb(Br/I)$_3$:Cd 40 mol % sample.

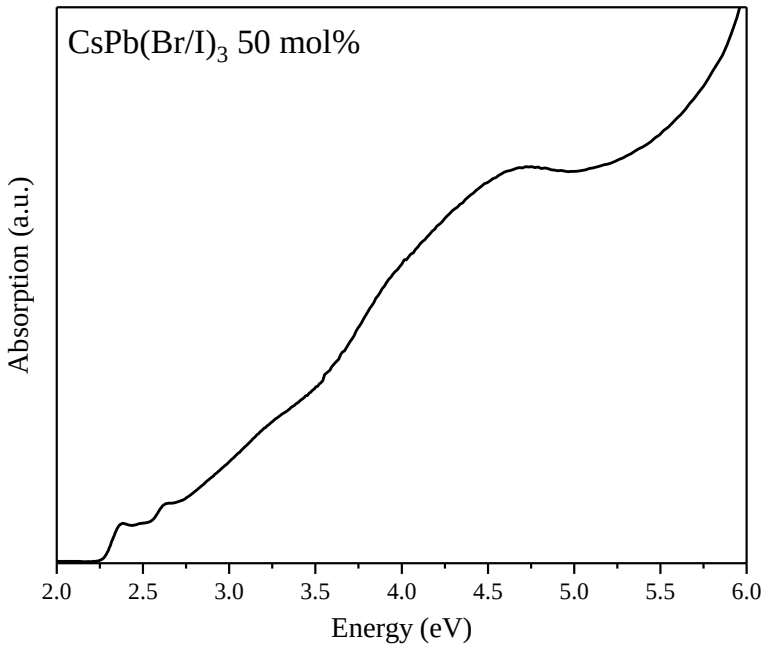

Figure 8.10 Absorption profile for the CsPb(Br/I)$_3$ 50 mol % sample.

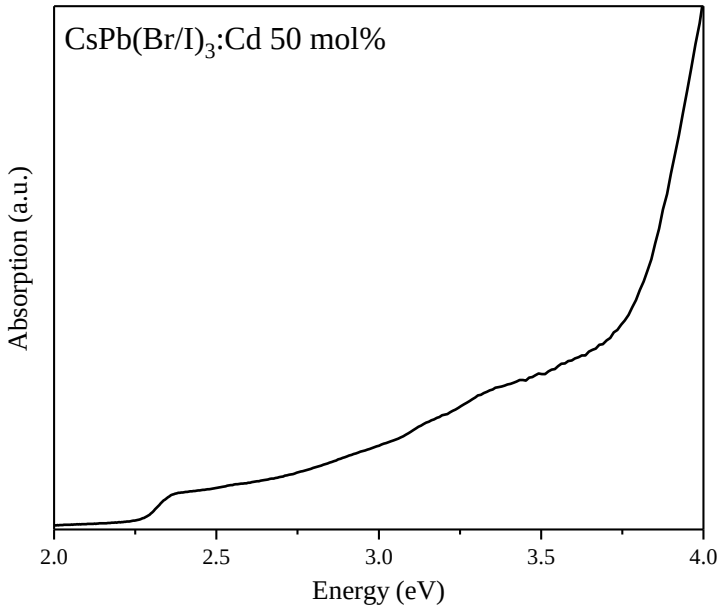

Figure 8.11 Absorption profile for the CsPb(Br/I)$_3$:Cd 50 mol % sample.

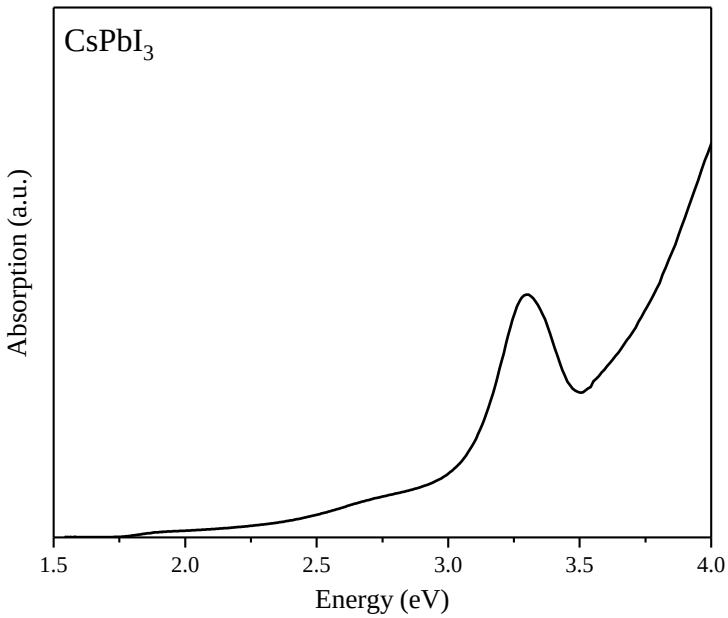

Figure 8.12 Absorption profile for the CsPbI$_3$ sample.

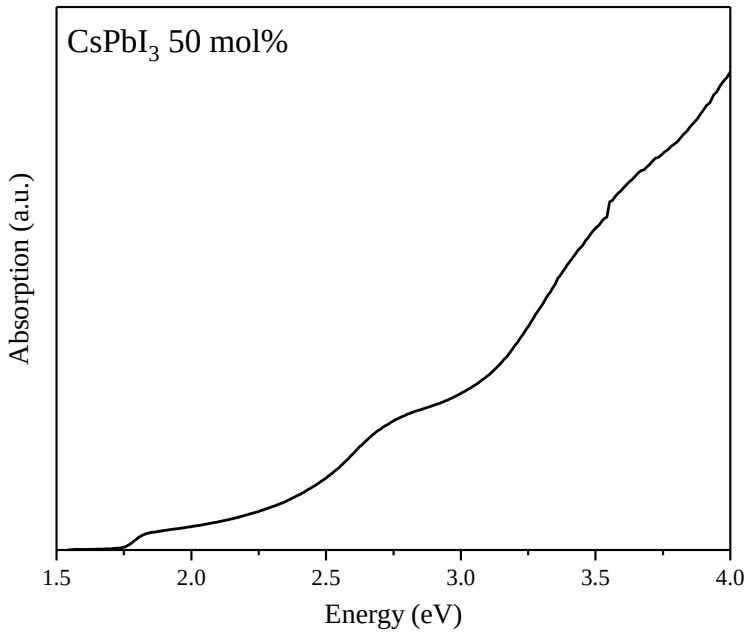

Figure 8.13 Absorption profile for the $CsPbI_3$:Cd 50 mol % sample.